Impact of model structure and parameterization on Penman-Monteith type evaporation models

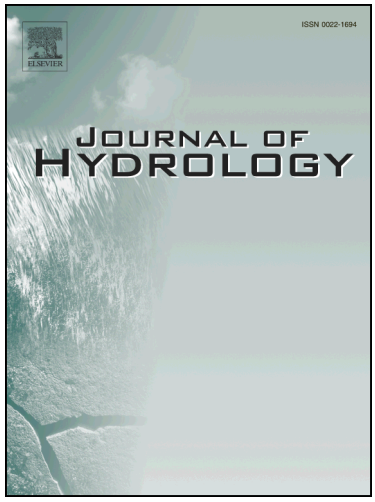

Impact of model structure and parameterization on Penman-Monteith type evaporation models

A. Ershadi, M.F. McCabe, J.P. Evans, E.F. Wood

PII: S0022-1694(15)00257-7
DOI: http://dx.doi.org/10.1016/j.jhydrol.2015.04.008
Reference: HYDROL 20367

To appear in: *Journal of Hydrology*

Received Date: 11 July 2013
Revised Date: 3 April 2015
Accepted Date: 5 April 2015

Please cite this article as: Ershadi, A., McCabe, M.F., Evans, J.P., Wood, E.F., Impact of model structure and parameterization on Penman-Monteith type evaporation models, *Journal of Hydrology* (2015), doi: http://dx.doi.org/10.1016/j.jhydrol.2015.04.008

Impact of model structure and parameterization on Penman-Monteith type evaporation models

A. Ershadi[a,#], M.F. McCabe[a], J.P. Evans[b], E.F. Wood[c]

[a] Division of Biological and Environmental Sciences and Engineering, King Abdullah University of Science and Technology (KAUST), Jeddah, Saudi Arabia

[b] ARC Centre of Excellence for Climate Systems Science and Climate Change Research Centre, University of NSW, Sydney, Australia

[c] Department of Civil and Environmental Engineering, Princeton University, Princeton, New Jersey, USA

[#] Corresponding author

Emails: Ali Ershadi (+966-(012)-8084970; ali.ershadi@kaust.edu.sa), Matthew McCabe (matthew.mccabe@kaust.edu.sa), Jason Evans (jason.evans@unsw.edu.au), Eric F. Wood (efwood@princeton.edu)

Abstract

The impact of model structure and parameterization on the estimation of evaporation is investigated across a range of Penman-Monteith type models. To examine the role of model structure on flux retrievals, three different retrieval schemes are compared. The schemes include a traditional single-source Penman-Monteith model (Monteith, 1965), a two-layer model based on Shuttleworth and Wallace (1985) and a three-source model based on Mu et al. (2011). To assess the impact of parameterization choice on model performance, a number of commonly used formulations for aerodynamic and surface resistances were substituted into the different

formulations. Model response to these changes was evaluated against data from twenty globally distributed FLUXNET towers, representing a cross-section of biomes that include grassland, cropland, shrubland, evergreen needleleaf forest and deciduous broadleaf forest.

Scenarios based on 14 different combinations of model structure and parameterization were ranked based on their mean value of Nash-Sutcliffe Efficiency. Results illustrated considerable variability in model performance both within and between biome types. Indeed, no single model consistently outperformed any other when considered across all biomes. For instance, in grassland and shrubland sites, the single-source Penman-Monteith model performed the best. In croplands it was the three-source Mu model, while for evergreen needleleaf and deciduous broadleaf forests, the Shuttleworth-Wallace model rated highest. Interestingly, these top ranked scenarios all shared the simple lookup-table based surface resistance parameterization of Mu et al. (2011), while a more complex Jarvis multiplicative method for surface resistance produced lower ranked simulations. The highly ranked scenarios mostly employed a version of the Thom (1975) formulation for aerodynamic resistance that incorporated dynamic values of roughness parameters. This was true for all cases except over deciduous broadleaf sites, where the simpler aerodynamic resistance approach of Mu et al. (2011) showed improved performance.

Overall, the results illustrate the sensitivity of Penman-Monteith type models to model structure, parameterization choice and biome type. A particular challenge in flux estimation relates to developing robust and broadly applicable model formulations. With many choices available for use, providing guidance on the most appropriate scheme to employ is required to advance approaches for routine global scale flux estimates, undertake hydrometeorological assessments or develop hydrological forecasting tools, amongst many other applications. In such cases, a multi-model ensemble or biome-specific tiled evaporation product may be an appropriate solution, given the inherent variability in model and parameterization choice that is observed within single product estimates.

Keywords: latent heat flux; evaporation; evapotranspiration; Penman-Monteith; surface resistance; aerodynamic resistance

1 Introduction

Accurate estimates of evaporation are required in water resources management, irrigation management and hydrologic studies. For this reason, a range of models have been developed to provide evaporation products across different spatial and temporal scales (Kalma et al., 2008; Wang and Dickinson, 2012). The Penman-Monteith (PM) model (Monteith, 1965) is one of the most widely employed approaches for the estimation of evaporation, as it has a process-based formulation that utilises commonly available meteorological variables, including air temperature, wind speed, humidity and radiation. The PM model forms the theoretical basis of a number of continental and global scale evaporation models (Ferguson et al., 2010; Mu et al., 2011) and land surface schemes (Chen and Dudhia, 2001), albeit with some variations in formulation and parameterization.

Underlying the performance of this common approach are important issues of model structure and parameterization that influence the utility of the technique for general application. In its simplest form, the Penman-Monteith model is a single-source “big-leaf” model that lumps the heterogeneity of the land surface into a single evaporative element. In this configuration, no distinction is made between evaporation from bare soil, evaporation from canopy intercepted water or transpiration via the canopy (processes encompassed herein via the term evaporation, following the definition in Kalma et al., 2008). However, other versions of the PM model have been developed that consider the land surface as a layered system (e.g. Shuttleworth and Wallace, 1985) or discriminate components of the land surface into different evaporative sources (e.g. soil and canopy), with a PM model formulated in each layer or component (e.g. Mu et al., 2011).

Inherent in the choice of model structure is the development and selection of appropriate parameterizations to describe the physical processes occurring within the system. In PM type

models, the aerodynamic (r_a) and surface resistance (r_s) schemes represent critical controls on heat and vapor flux transfer through the soil, plant and atmospheric continuum. Given the importance of the resistance parameterization in flux estimation (McCabe et al., 2005), a number of studies have examined various resistance parameterization techniques in PM type models. The underlying assumption in many of these studies has been that if the resistance parameters are estimated accurately, then the (single-source) PM type model should be able to provide an accurate estimate of evaporation (Raupach and Finnigan, 1988). Of course, the challenge is that direct independent measurement of resistances is difficult, so discriminating good parameterizations from bad is not trivial.

In addition to uncertainties that originate from inadequate surface resistance and aerodynamic resistance formulations, the single-source structure of the PM model can also cause errors in estimating evaporation. In terms of model structure, the single-source PM model was originally developed for the special case of a dense, well-watered canopy that absorbs most of the available energy. However, in sparse canopies, evaporation from the soil can be as important as the canopy transpiration (Shuttleworth and Wallace, 1985). In these scenarios, the partitioning of total evaporation to different sources or layers is important (Allen et al., 2011). Furthermore, the "big-leaf" assumption requires that the sources of heat and water vapour occur at the same level within the canopy (Finnigan et al., 2003; Foken et al., 2012). This requirement might be met in a short and dense canopy or a bare soil surface, but is unlikely to be true for a tall or sparse canopy (Wallace, 1995).

As a consequence of these limitations and a desire to develop approaches with more general or universal application, a number of efforts have been directed towards improving the structure of the single source PM model to multi-layer or multi-source schemes. In a multi-layer scheme, the representation of the soil-canopy-atmosphere system is improved by vertically dividing the canopy structure into separate layers, with each utilizing the PM model, but linked via a network of

resistances. Such a multi-layer configuration means that the resistances are coupled in series and have interactions (Shuttleworth and Wallace, 1985; Choudhury and Monteith, 1988). In multi-source schemes, the total evaporation from the land surface is generally partitioned into evaporation from the soil, transpiration from the canopy and evaporation from the intercepted water in the canopy (with the latter absent in two-layer schemes). In contrast to multi-layer schemes, multi-source schemes have resistances that are often in parallel and hence have no interaction.

Relatively few studies have focused on an intercomparison of PM based models to evaluate the significance and effectiveness of both the model structure and the choice of parameterization (Stannard, 1993; Huntingford et al., 1995; Fisher et al., 2005). In reviewing the literature it is readily apparent that there are few definitive outcomes with which to guide the selection of the most appropriate model configuration for a particular land surface. A missing element of many previous efforts was a comprehensive examination of model and data characteristics, such as the role of model structure (e.g. single-source, multi-layer, multi-source), impact of model parameterizations (e.g. resistances and roughness) and variability in climate zone and biome type (e.g. grassland, cropland, forest). Furthermore, most studies were performed over relatively short periods of weeks to months (e.g. Stannard, 1993; Huntingford et al., 1995) as a consequence of data limitations, with few cases extending into yearly time periods (e.g. Fisher et al., 2005; Ortega-Farias et al., 2010). Clearly, multi-year datasets are better able to represent the dynamics in the bio-physiological and hydro-meteorological variability of the land surface: issues that are central in evaporation estimation and comprehensive model evaluation.

These issues provide the motivation to evaluate the role of model structure and parameterization across a range of PM type models. For this purpose, we selected three model structures: the original single-source Penman-Monteith model (Monteith, 1965), a modified two-layer model (Shuttleworth and Wallace, 1985) and a three-source model (Mu et al., 2011). Each scheme was then adjusted to incorporate a variety of aerodynamic and surface resistance parameterizations. To maintain a

realistic range of land surface dynamics, we used a globally distributed set of eddy-covariance towers that contain (relatively) long periods of data. These in-situ measurements provide the needed meteorological forcing to drive the different schemes and the observed heat flux data required to evaluate the model simulations. Our model assessment and intercomparison exercise is used to address the following research questions: What is the significance of model structure in the performance of Penman-Monteith type models? What is the relative significance of aerodynamic and surface resistances? Which of the model structures and parameterizations are most appropriate for the accurate estimation of evaporation over different landscapes and biome types?

2 Data and Methodology

2.1 Input Forcing and Evaluation Data

The data used for the development and evaluation of the models in this study comprise of 20 globally distributed eddy-covariance towers from the FLUXNET project (Baldocchi et al., 2001). While there are more than 500 towers available from this data archive, a limiting factor on tower selection was the need for soil moisture data for calculations of the surface resistance (see Section 2.3.1). As this variable is not monitored routinely at most tower sites, the capacity for more extensive tower based assessment was significantly reduced. The selected towers are distributed across a range of biome types that include grassland, cropland, shrubland, evergreen needleleaf forest and deciduous broadleaf forest. In each of these biomes, four towers were selected, each with a different canopy height. The period of data across the selected towers varies from 1.5 to 10 years at either hourly or half-hourly time steps, effectively capturing the required variability in canopy development and hydrometeorological conditions. All data were filtered for daytime only measurements, which was defined as when the shortwave downward radiation was greater than 20 $W.m^{-2}$. This criterion also filters early morning and late afternoon transitions in the atmospheric boundary layer. The data were also filtered for rain events, for frozen periods (when air or land temperature is equal or below

zero), for negative turbulent fluxes, for gap-filled records and for low-quality control flags (i.e. quality flag = 0). In total, more than 100 site-years of data (or approximately 500,000 filtered records) were processed for each model formulation. Attributes of the selected towers are listed in Table A1 and a map of the tower locations is provided in Figure 1.

Figure 1

2.2 Satellite Based Vegetation Data

Phenological characteristics of vegetation, such as the leaf area index and fractional vegetation cover, are required for the parameterization of aerodynamic and surface resistances. As in-situ vegetation data are not generally available at the tower sites, an alternative is to estimate vegetation indices and parameters from remote sensing data. Here, we use remote sensing products from the Moderate-Resolution Imaging Spectroradiometer (MODIS) sensor, which have been employed for this purpose in a number of previous investigations (e.g. Fisher et al., 2008; Mu et al., 2011). We also use a time series of the Normalized Difference Vegetation Index (NDVI) based on the MODIS MOD13Q1 product (Solano et al., 2010) at 250 m spatial resolution and 16 day temporal frequency for the pixel containing each tower. A 3x3 window has been used in other evaporation studies to reduce geo-location errors (Wolfe et al., 2002) and gridding artefacts (Tan et al., 2006) that may present in single-day or 8-day products. While a single pixel is expected to better match the footprint of the eddy-covariance towers, comparison of NDVI derived from a single pixel versus a 3x3 window showed a high level of agreement, with an average coefficient of determination (R^2) of 0.96 and a root-mean-square difference (RMSD) of 0.03 when averaged across all towers.

NDVI time series were obtained from the Simple Object Access Protocol (SOAP) web service of the Oak Ridge National Laboratory (ORNL) MODIS Land Product Subsets (http://daac.ornl.gov/MODIS/). Gaps in the NDVI records were filled by a simple linear interpolation between the 16 day retrievals. Given the reliance on satellite data, the tower records coincide with the start of the MODIS record in the year 2000. The gap-filled NDVI time series was converted to leaf area index (LAI) using the

171 methodology developed by Ross (1976), with coefficients from Fisher et al. (2008). The fractional
172 vegetation cover was calculated using the methodology presented by Jiménez-Muñoz et al. (2009). A
173 summary of statistics for the fractional vegetation cover and LAI at tower sites is provided in Table
174 S1 of the Supplementary Materials.

175 2.3 Description of Penman-Monteith Model Structures

176 Following is a description of each of the models examined in this analysis, along with the default
177 resistance schemes that comprise the implemented version of the model. While the model
178 formulations are described herein, the reader is referred to Appendices B to D and the provided
179 principal model references for further details.

180 2.3.1 Single-source Penman-Monteith (PM) model

181 The Penman model (Penman, 1948) was originally developed for the estimation of the potential
182 evaporation from open water and saturated land surfaces. To generalize the Penman equation for
183 water-stressed crops, Monteith (1965) incorporated a canopy resistance term to describe the effect
184 that partially closed stomata have on evaporation (Inclán and Forkel, 1995). The PM model
185 conceptualizes the land surface as a so-called "big-leaf", describing the land surface-atmosphere
186 exchange via a single bulk stomatal resistance and a single aerodynamic resistance to heat and
187 vapour. The PM model for estimation of actual evaporation can be formulated as follows (Brutsaert,
188 2005):

$$\lambda E = \frac{\Delta A + \rho c_p (e^* - e)/r_a}{\Delta + \gamma(1 + \frac{r_s}{r_a})} \qquad 1$$

189 where λE is actual evaporation in W.m^{-2}, λ is the latent heat of vaporization (2.43 × 10^6 J.kg^{-1})
190 , Δ is the slope of the saturation water vapour pressure curve at an air temperature T_a, ρ is air
191 density (m^3.kg^{-1}), γ is the psychrometric constant defined as $\gamma = c_p P_a/(0.622\lambda)$ with c_p being
192 specific heat capacity of air (J.kg^{-1}.K^{-1}), and P_a is the air pressure in Pa. $e^* - e$ is the vapor pressure

193 deficit, with e^* the saturation vapour pressure and e the actual vapor pressure of the surrounding air
194 (both in Pa). The aerodynamic and surface resistance parameters (r_a and r_s) are in units of s.m^{-1}. A is
195 the available energy, defined as $A = R_n - G_0$ with R_n and G_0 describing the net radiation and
196 ground heat flux respectively.

197 The aerodynamic resistance formulation used in the standard PM model of this study is that of Thom
198 (1975) (hereafter Thom's equation):

$$r_a = \frac{1}{\kappa^2 u_a}\left[\ln\left(\frac{z-d_0}{z_{0m}}\right)\ln\left(\frac{z-d_0}{z_{0v}}\right)\right] \quad \textbf{2}$$

199 where z is measurement height (m), u_a is wind speed (m.s^{-1}), $\kappa = 0.41$ is von Karman's
200 constant, d_0 is displacement height and z_{0m} and z_{0v} are the roughness heights for momentum and
201 water vapor transfer respectively (all in meters). Following Brutsaert (2005), we assume $z_{0v} = z_{0h}$
202 with z_{0h} being the roughness height for heat transfer. It is common practice to use roughness
203 parameters (d_0, z_{0m}, z_{0h}) with static values calculated as a fraction of the canopy height (h_c), so
204 here we employ the equations suggested by Brutsaert (2005):

$$\begin{aligned} d_0 &= 0.66h_c \\ z_{0m} &= 0.1h_c \\ z_{0h} &= 0.01h_c \end{aligned} \quad \textbf{3}$$

205 For the estimation of the surface resistance, the Jarvis scheme of Jacquemin and Noilhan (1990)
206 (hereafter Jarvis method) is used (see Appendix B).

207 ### 2.3.2 Two-layer Shuttleworth-Wallace (SW) model

208 The Penman-Monteith model was extended to a two-layer configuration by Shuttleworth and
209 Wallace (1985) (SW) that included separate canopy and soil layers. The total evaporation in the SW
210 model is $\lambda E = C_c PM_c + C_s PM_s$, where C_c and C_s are resistance functions for canopy and soil
211 (respectively). PM_c and PM_s are terms that represent the Penman-Monteith equation applied to full
212 canopy and to bare soil:

$$PM_c = \frac{\Delta A + \frac{\rho c_p (e^* - e) - \Delta r_a^c A_s}{r_a^a + r_a^c}}{\Delta + \gamma [1 + r_s^c / (r_a^a + r_a^c)]} \quad (4)$$

$$PM_s = \frac{\Delta A + \frac{\rho c_p (e^* - e) - \Delta r_a^s (A - A_s)}{r_a^a + r_a^s}}{\Delta + \gamma [1 + r_s^c / (r_a^a + r_a^c)]} \quad (5)$$

where A is the available energy for the complete canopy ($A = R_n - G_0$) and A_s is the available energy at the soil surface ($A_s = R_n^s - G_0$)). R_n^s is net radiation at the soil surface, which can be calculated using Beer's law as $R_n^s = R_n \exp(-C \cdot LAI)$, with $C = 0.7$ representing the extinction coefficient of the vegetation for net radiation. The resistance parameters in the SW model include bulk canopy resistance (r_s^c), soil surface resistance (r_s^s), aerodynamic resistance between soil and canopy (r_a^s), canopy bulk boundary layer resistance (r_a^c) and aerodynamic resistance between the canopy source height and a reference level above the canopy (r_a^a). In application of the SW model, r_a^a and r_a^s are calculated using the methodology by Shuttleworth and Gurney (1990) (hereafter SG90). Details of the SW model formulation, as well as the standard parameterization of the resistances used in this study are detailed in Appendix C.

2.3.3 Three-source Mu et al. (2011) (Mu) model

The three-source PM model used in this investigation is based on that developed by Mu et al. (2011). In the Mu model, total evaporation is partitioned into evaporation from the intercepted water in the wet canopy (λE_{wc}), transpiration from the canopy (λE_t) and evaporation from the soil (λE_s), defined as $\lambda E = \lambda E_s + \lambda E_t + \lambda E_{wc}$. Evaporation for each source component is derived from the PM equation and weighted based on fractional vegetation cover (f_c), relative surface wetness (f_w) and available energy. Parameterization of aerodynamic and surface resistance for each source is based on biome specific (constant) values of leaf and stomatal conductances for water vapor and sensible heat transfer, scaled by vegetation phenology and meteorological variables. From a forcing data perspective, one advantage of the resistance parameterization in the Mu model is that it does not

require wind speed and soil moisture data: two variables that are often difficult to prescribe accurately. Specific details of the model formulation are provided in Appendix D.

2.4 Inclusion of a Dynamic Roughness Parameterization

In addition to assuming roughness parameters (d_0, z_{0m}, z_{0h}) as a constant fraction of the canopy height (i.e. static roughness) as detailed above, these variables can also be estimated via a physically-based method. Su et al. (2001) used vegetation phenology, air temperature and wind speed to provide dynamic values of roughness parameters based on the land surface condition. Details of this method are provided in Appendix E.

2.5 Developing Model Parameterization Scenarios

To examine the influence of resistance schemes and model structure on flux simulations, we developed fourteen unique scenarios. Details of these distinct combinations are provided in Table 1. For the default model implementations described above (denoted here as PM^0, SW^0 and Mu^0), parameterizations of the aerodynamic and surface resistances are not modified. For each model type, alternative scenarios are developed to examine the influence of aerodynamic and surface resistance parameterization (see Appendices B to E) and are denoted by superscripts 1, 2, 3, 4 (e.g. PM^1, PM^2). For example, a comparison of PM^0 and PM^1 (see Table 1) illustrates the effect of changing the surface resistance parameterization only, while comparison of PM^0 and PM^2 show the effect of changing the aerodynamic resistance parameterization only (via a change in roughness parameterization). PM^3 and PM^4 show the combined effect of both aerodynamic and surface resistances. In a similar vein for the SW model, comparison of SW^0 and SW^1 isolates the effect of changing the surface resistance parameterization only, while comparison of SW^0 and SW^2 shows the effect of changing the aerodynamic resistance parameterization only. SW^3 and SW^4 are similar to those of PM^3 and PM^4. For the Mu model, three alternative scenarios are considered to examine the effects of changing aerodynamic resistance (with static and dynamic roughness) and surface

resistance. Table S3 in the Supplementary Materials lists the forcing variables that are required to run each case of the resistance parameterizations.

Table 1: Features of the fourteen model parameterisation combinations for estimating evaporation, where r_s is the surface resistance and r_a is the aerodynamic resistance (see Section 2.3 and Appendices B to D for model and parameterization details).

Scenario	Model	r_s	r_a	Roughness
PM^0	PM	Jarvis	Thom	static
PM^1	PM	Mu	Thom	static
PM^2	PM	Jarvis	Thom	Dynamic
PM^3	PM	Mu	Thom	Dynamic
PM^4	PM	Mu	Mu	N/A
SW^0	SW	Jarvis	SG90	static
SW^1	SW	Mu	SG90	static
SW^2	SW	Jarvis	Thom	Dynamic
SW^3	SW	Mu	Thom	Dynamic
SW^4	SW	Mu	Mu	N/A
Mu^0	Mu	Mu	Mu	N/A
Mu^1	Mu	Mu	Thom	Dynamic
Mu^2	Mu	Mu	Thom	static
Mu^3	Mu	Jarvis	Mu	N/A

2.6 Statistical Evaluation of Model Response

We used the R^2, *RMSD*, the relative error (*RE*) and the Nash-Sutcliffe efficiency (*NSE*) coefficient for statistical evaluation of the model intercomparison and parameterization scenarios. The relative error is defined as the RMSD normalized by the mean value of the observed evaporation ($\overline{\lambda E_{obs}}$), i.e. $E = RMSD/\overline{\lambda E_{obs}}$, which is used in a number of similar studies (Su et al., 2005; Kalma et al., 2008). The *NSE* is a normalized statistic that determines the relative magnitude of the residual variance (noise) compared to the variance of the measured response (Nash and Sutcliffe, 1970) and defined as:

$$NSE = 1 - \left[\frac{\sum_{i=1}^{n}\left(\lambda E_{i,obs} - \lambda E_{i,sim}\right)^2}{\sum_{i=1}^{n}\left(\lambda E_{i,obs} - \overline{\lambda E_{obs}}\right)^2}\right] \quad (6)$$

where $\lambda E_{i,obs}$ is the ith observed λE, $\lambda E_{i,sim}$ is the ith simulated λE and n is the total number of observations. The *NSE* coefficient is an indicator of linear fit to the scatterplot of observed versus simulated data to the 1:1 line. This coefficient has a range between $-\infty$ and 1.0, with an *NSE*=1 indicating an optimal value. Generally, *NSE* values that are in the range 0 to 1 describe acceptable modelling performance, whereas negative *NSE* values indicate poor performance (Moriasi et al., 2007). The NSE_{avg}, R^2_{avg} and RE_{avg} are used in this paper to represent the average values of the statistics for multiple towers, and NSE_{std} is used to calculate the standard deviation of *NSE* for multiple towers. Hourly or half-hourly filtered data (dependent on the forcing data source) were used together with the model-simulated responses to calculate these statistical measures.

It should be noted that measurement uncertainty in observed tower fluxes is not explicitly included in these analyses. As such, some caution is required in their interpretation, especially when evaporation is low and measurement uncertainty might equal the modelling uncertainty. Furthermore, the issue of non-closure implicit in the eddy-covariance approach (Twine et al., 2000) can increase the uncertainty in observations. The issue was evaluated in Ershadi et al. (2014) through examining the energy residual and the Bowen-ratio closure methods using the same towers employed herein. Ershadi et al. (2014) found that the energy residual closure correction technique provided better agreement with modelling results and therefore that approach has been adopted here.

3 Results

Plots of R^2, *RE* and *NSE* for the modelling scenarios are provided in the following sections. Evaluation of the different scenarios focuses mainly on the *NSE* of individual towers or on the NSE_{avg} as a representative value for a biome (see Table 2), as neither the R^2 as a correlation metric nor the *RE* as

a bias error metric are suited as stand-alone measures of scenario performance. For example, a model may show a high R^2, but with large slope or y-intercept for the linear regression (e.g. Figure S8 in the Supplementary Materials). Nevertheless, scatterplots and the statistical metrics are provided for each simulation scenario and each tower site in the Supplementary Materials.

3.1 Penman-Monteith Model

Influence of r_s parameterization: The impact of changing the surface resistance scheme from the standard Jarvis method (Equation B1) in PM^0, to that used in the Mu model (Equation D6) in PM^1 is shown in Figure 2 (the equivalent bar plot can be found in Figure S16 of the Supplementary Materials). A key assumption in the surface resistance parameterization of the Mu model is that the near-surface humidity reflects variations in the soil moisture and hence a humidity-index can be substituted for soil-water stress (Fisher et al., 2008). If this approach can be shown to provide a good representation of the surface resistance, it would remove the reliance on the use of error-prone soil moisture data in calculating this parameter. Based on the *NSE*, an improved modelling performance is observed for most towers relative to the standard Jarvis method, excluding G1, E2, D1, D2 and D3 sites. From PM^0 to PM^1, the change in NSE_{avg} (i.e. the mean *NSE* of multiple towers) is positive for grasslands (0.34→0.50), for croplands (0.24→0.53), for shrublands (0.12→0.29) and for evergreen needleleaf forest (0.09→0.21), but negative for deciduous broadleaf forest sites (0.40→0.36). Amongst grassland, cropland, shrubland and evergreen needleleaf forest biomes, the improvement in *NSE* is more evident for cropland sites, where the range in *NSE* is increased from 0.07-0.44 to 0.42-0.65 and the range in *RMSD* is reduced from 107-126 $W.m^{-2}$ to 75-103 $W.m^{-2}$ (see Figures S1, S4, S7, S10 and S13 in the Supplementary Materials for statistics). Comparison of PM^2 with PM^3 (changing Jarvis r_s to Mu r_s) confirms a similar response of trends in NSE_{avg} across the biomes.

Influence of r_a parameterization: The influence of dynamic versus static roughness on modelling performance can be tracked in comparisons of two sets of scenarios: PM^2 and PM^0, and PM^3 and PM^1. In PM^2, adjusting the aerodynamic resistance parameterization via the use of dynamic

roughness values only improved modelling performance slightly when compared to PM^0. This improvement (in terms of NSE_{avg}) is more evident for croplands (0.24→0.38) and for deciduous broadleaf forest sites (0.40→0.64). Improvements in NSE_{avg} from PM^0 to PM^2 are smaller for grasslands (0.34→0.40), shrublands (0.12→0.16) and for evergreen needleleaf forest (0.09→0.20). Likewise, comparing PM^3 with PM^1 shows that the *NSE* at all towers is increased. The results from both sets of scenarios show the positive effect of adding dynamic roughness to the single-source PM model structure.

The PM^4 is designed to investigate whether the simple lookup-table based aerodynamic parameterization of the Mu model (equation D11) can be used in the single-source PM model. The benefit of this approach is that the method does not require either roughness parameters or wind speed. Comparison of *NSE* values of the PM^4 with those of the PM^3 shows that *NSE* at most towers is decreased in PM^4, except in deciduous broadleaf forest sites. Therefore, use of the lookup table based approach of Mu for r_a parameterization is not recommended if wind and canopy height data are available. However, comparison of PM^4 and PM^0 shows that in cases where wind, canopy height and soil moisture data are not available, use of the Mu based r_a and r_s parameterizations can increase *NSE* at most sites, excluding G1, G3, S2 and E2 sites. This is an important result, as these variables are the ones that are most often unavailable in data poor regions.

The best performing PM scenario: Overall, the PM^3 (which uses Mu r_s and Thom r_a) provides the best performance across most biomes, except over deciduous broadleaf forest sites where PM^2 (which uses Jarvis r_s and Thom r_a) presents the best outcome. Both PM^3 and PM^2 utilise Thom's equation with dynamic roughness, which requires reliable wind speed and canopy height data. Results also suggest that the Jarvis method (used in PM^2) is suitable for deciduous broadleaf forest sites, but for other biomes the simpler Mu model resistance (used in PM^3) is more suitable.

Figure 2

3.2 Shuttleworth-Wallace Model

Influence of r_s parameterization: Figure 3 and its equivalent bar plot (see Figure S17 in the Supplementary Materials) illustrate variations of R^2, *RE* and *NSE* coefficients for the different SW scenarios. A change in surface resistance from Jarvis to Mu in SW^0 to SW^1 had a limited influence on evaporation estimation over grassland sites (NSE_{avg} remained constant at 0.43), but improved the NSE_{avg} for cropland (0.08→0.36), evergreen needleleaf forest (-0.04→0.08) and deciduous broadleaf forest sites (-0.37→0.17) and decreased it for shrublands (0.07→0.02).

The effect of change in r_s parameterization from Jarvis to Mu can also be evaluated by comparing SW^2 and SW^3 (which share Thom r_a with dynamic roughness). The comparison in terms of NSE_{avg} shows a similar trend (as observed for SW^0 to SW^1) for cropland (0.43→0.48) and for evergreen needleleaf forest sites (0.20→0.38), but different trends across grassland (0.44→0.29), shrubland (0.17→0.21) and deciduous broadleaf forest sites (0.65→0.66). The results identify that for the SW model, the influence of r_s parameterization is impacted by the influence of the choice of r_a parameterization. As such, parameterizing resistances for the SW model should be undertaken with care. Overall, a change in surface resistance had less impact on the modelling efficiency of the SW model structure when compared to that observed for the single-source PM model (see Figure 2).

Influence of r_a parameterization: For aerodynamic resistance, comparisons include evaluating the impact of changes from the SG90 r_a to the Thom r_a with dynamic roughness (SW^0 → SW^2 and SW^1 → SW^3), from SG90 r_a to the Mu r_a (SW^1 → SW^4), and from Thom r_a with dynamic roughness to Mu r_a (SW^3 → SW^4).

Compared to SW^0, employing Thom's equation with dynamic roughness in SW^2 slightly improved the NSE_{avg} for grasslands (0.43→0.44), considerably increased it for cropland (0.08→0.43), shrubland (0.07→0.17) and evergreen needleleaf forest sites (-0.04→0.20) and dramatically improved it for deciduous broadleaf forest sites (-0.37→0.65). The larger positive response to the changes in r_a

parameterization in the cropland and the deciduous broadleaf forest sites can be related to the structure of those canopies. That is, the Thom r_a equation with dynamic roughness is better able to represent the aerodynamic transfer processes when full canopy and soil/understory layers are vertically represented and interact in series as in the SW model structure.

For application of the Mu r_a in the SW model, comparison of SW^1 (Mu r_s, SG90 r_a) with SW^4 (Mu r_s, Mu r_a) shows that the NSE_{avg} is decreased for grasslands (0.43→0.04) and shrublands (0.02→-0.04), remained constant at 0.36 for croplands, but is significantly increased for evergreen needleleaf forest sites (0.08→0.24) and for deciduous broadleaf forest sites (0.17→0.76). Also, a change of Thom r_a with dynamic roughness in SW^3 to Mu r_a in SW^4 confirms a decrease in NSE_{avg} for a majority of the towers, except for deciduous broadleaf forest sites where it increases (0.66→0.76).

Overall, Thom r_a with dynamic roughness (used in SW^2 and SW^3) performed best over grassland, cropland, shrubland and evergreen needleleaf forest sites, while Mu r_a performed best over deciduous broadleaf forest sites.

Influence of using Mu resistance parameterizations: Comparison of SW^4 and SW^0 was designed to identify whether a simpler and less data demanding resistance parameterization (i.e. using both r_s and r_a from the Mu model) can be usefully employed in flux estimation. Results show that such a parameterization is effective in increasing the NSE_{avg} across deciduous broadleaf forest sites (-0.37→0.76), evergreen needleleaf forest sites (-0.04→0.24) and croplands (0.08→0.36). However, the performance is degraded across grasslands (0.43→0.04) and shrublands (0.07→-0.04). As such, the use of the SW^4 configuration is not advised for grasslands and shrublands.

The best performing SW scenarios: Amongst the studied biomes, the SW^2 has the best performance over grasslands (marginal improvement over SW^0 and SW^1), while SW^4 has the best performance over deciduous broadleaf forest sites. For other biomes, SW^3 is the best option. The use of the Mu surface resistance in SW^3 and SW^4 relaxes the need for soil moisture data. In contrast, the use of the

Jarvis surface resistance in SW^2 demands reliable soil moisture data. Also, application of the Mu r_a parameterization for deciduous broadleaf forest sites in SW^4 removes the need for wind and canopy height data. However, accurate wind speed and canopy height data are required for SW^2 and SW^3, both of which use Thom r_a.

Figure 3

3.3 Mu Model

Influence of r_a parameterization: Figure 4 and its equivalent bar plot (see Figure S18 in the Supplementary Materials) indicate that from Mu^0 to Mu^1 the NSE_{avg} is increased for grassland (0.43→0.47), cropland (0.65→0.67), shrubland (0.10→0.18) and evergreen needleleaf forest sites (0.30→0.35), but is decreased for deciduous broadleaf forest sites (0.71→0.66). As such, Thom r_a with dynamic roughness slightly improves the performance of the model, except over deciduous broadleaf forest sites. Comparison of Mu^0 to Mu^2 (changing Mu r_a to Thom r_a with static roughness) shows a similar response of trends in NSE_{avg}, but smaller in magnitude, across the biomes. These results suggest that the change in aerodynamic resistance in the Mu model has a relatively small influence on the modelling performance, except for deciduous broadleaf forest sites.

Influence of r_s parameterization: Compared to Mu^0, which uses the Mu surface resistance, application of the Jarvis surface resistance in the Mu^3 produced lower values of *NSE*, except for S1, E2 and D1 towers. In particular, the NSE_{avg} is decreased over croplands (0.65→0.50) and evergreen needleleaf forest sites (0.30→0.15). However, change in NSE_{avg} was marginal over deciduous broadleaf forest sites (0.71→0.70). Overall, the use of Mu r_s provides more robust flux estimation than does the use of the Jarvis method over a majority of the studied biomes. Such findings are important in the application of the Mu model in data sparse regions, where accurate soil moisture data are not available.

The best performing Mu scenario: The Mu^1 scenario has the highest NSE_{avg} over grassland, cropland, shrubland and evergreen needleleaf forest sites, and the Mu^0 has the highest NSE_{avg} for deciduous broadleaf forest sites. When accurate wind speed data or roughness parameters are not available, Mu^0 can be used as a replacement for Mu^1 with a small compromise in estimation efficiency, as the changes in NSE_{avg} from Mu^0 to Mu^1 were relatively small. Mu^0 also performed better than Mu^3 (Jarvis r_s, Mu r_a), except over deciduous broadleaf forest sites where the performance was similar.

Figure 4

Table 2: NSE_{avg} values of all scenarios over various biomes, with the standard deviation of *NSE* values shown in parenthesis. Values in the shaded cells identify the top-ranked scenarios for each biome. Biomes shown in the first column include grassland (GRA), cropland (CRO), shrubland (SHR), evergreen needleleaf forest (ENF) and deciduous broadleaf forest (DBF).

Biome	Model	Scenario				
		0	1	2	3	4
GRA	PM	0.34 (0.43)	0.50 (0.23)	0.40 (0.40)	0.53 (0.23)	0.44 (0.22)
	SW	0.43 (0.34)	0.43 (0.34)	0.44 (0.36)	0.29 (0.41)	0.04 (0.50)
	Mu	0.43 (0.29)	0.47 (0.29)	0.46 (0.29)	0.37 (0.29)	(N/A)
CRO	PM	0.24 (0.18)	0.53 (0.12)	0.38 (0.19)	0.57 (0.12)	0.55 (0.12)
	SW	0.08 (0.36)	0.36 (0.25)	0.43 (0.18)	0.48 (0.23)	0.36 (0.29)
	Mu	0.65 (0.13)	0.67 (0.11)	0.64 (0.11)	0.50 (0.09)	(N/A)
SHR	PM	0.12 (0.07)	0.29 (0.12)	0.16 (0.10)	0.35 (0.15)	0.19 (0.10)
	SW	0.07 (0.03)	0.02 (0.25)	0.17 (0.10)	0.21 (0.35)	-0.04 (0.21)
	Mu	0.10 (0.08)	0.18 (0.14)	0.15 (0.11)	0.04 (0.03)	(N/A)
ENF	PM	0.09 (0.18)	0.21 (0.19)	0.20 (0.19)	0.29 (0.23)	0.19 (0.19)
	SW	-0.04 (0.20)	0.08 (0.19)	0.20 (0.19)	0.38 (0.19)	0.24 (0.16)
	Mu	0.30 (0.25)	0.35 (0.27)	0.31 (0.26)	0.15 (0.19)	(N/A)
DBF	PM	0.40 (0.15)	0.36 (0.10)	0.64 (0.06)	0.52 (0.11)	0.60 (0.10)
	SW	-0.37 (0.54)	0.17 (0.15)	0.65 (0.06)	0.66 (0.08)	0.76 (0.05)
	Mu	0.71 (0.09)	0.66 (0.10)	0.54 (0.11)	0.70 (0.07)	(N/A)

3.4 Identification of the Best Performing Models and Parameterizations

To develop an overall understanding on the performance of the reviewed scenarios, the NSE_{avg} and NSE_{std} of each scenario for each biome were calculated (see Table 2). From this table it can be seen that the best performing scenario for grassland and shrubland sites is PM[3], for croplands it is Mu[1], for evergreen needleleaf forest sites it is SW[3] and for deciduous broadleaf forest sites it is SW[4]. In all of these scenarios (PM[3], Mu[1], SW[3], SW[4]) the surface resistance is based on the Mu method, which requires no soil moisture data. Of the selected top performing scenarios, the Mu r_a method is only used in SW[4] (best performing in the deciduous broadleaf forest sites). However, in the PM[3], SW[3] and Mu[1] scenarios the aerodynamic resistance is calculated using Thom's equation with dynamic roughness, which requires reliable wind and canopy height data. As these forcing data are not always available for large-scale applications, an important question is to determine whether the scenarios that use Mu r_a over grassland, cropland, shrubland and evergreen needleleaf forest sites can produce NSE_{avg} values close to the top performing model?

To answer this, inspection of the NSE_{avg} and NSE_{std} values in Table 2 shows that for croplands, Mu[0] satisfies the above constraint (0.65 compared to 0.67 for the top model). However, for grassland sites the next best scenario is PM[1] (NSE_{avg} = 0.50), which relies on the Thom r_a formulation. Likewise, no highly ranked alternative scenario can be found for the shrubland and evergreen needleleaf forest sites. As such, there are no alternative candidate scenarios for grassland, shrubland and evergreen needleleaf forest biomes that produce NSE_{avg} values comparable to those realized from the top-performing scenarios (see Table 2) by substituting the Mu r_a in the models.

4 Discussion

In the present study, fourteen different scenarios were constructed to examine how changes in the default resistance parameterizations of a single-source, a two-layer and a three-source PM type model might influence their performance in the reproduction of actual evaporation.

Intercomparison of these scenarios provided insights into the influence of both model structure and parameterizations.

4.1 Impact of Changes in Model Structure

Influence of r_a parameterization: The aerodynamic resistance played a relatively minor role in flux estimation for the PM model, in accord with the findings of Bailey and Davies (1981) and Irmak and Mutiibwa (2010). Likewise, changes in the aerodynamic resistance in the Mu scenarios produced only minor improvements in model performance. In contrast, parameterization of the aerodynamic resistance had a major influence on the performance of the SW scenarios. Comparison of the various r_a schemes in the PM, SW and Mu models indicated that while the Thom r_a with dynamic roughness, which requires wind speed and canopy height data, increased the NSE_{avg} over a majority of the studied biomes, the performance advantage relative to using the Mu r_a was generally marginal for the PM and Mu models. Where wind speed and canopy height data are available, Thom r_a with dynamic roughness is recommended for the SW model, except over the deciduous broadleaf forest biome.

Influence of r_s parameterization: Analysis of the scenarios illustrated that the surface resistance parameterization significantly affects model performance in the PM and Mu models, while the SW models showed variable responses. For the PM scenarios, the Mu r_s increased the overall performance (i.e. NSE_{avg}) in croplands, and to a lesser extent in shrubland, evergreen needleleaf forest and in grassland sites. However, it did not improve the results in the deciduous broadleaf forest sites. The response of the Mu model to a change in surface resistance parameterization was somewhat different. In the Mu scenarios, the default r_s parameterization performed better than that of the Jarvis method, except over deciduous broadleaf forest sites where the performance change was marginal. Nevertheless, pre-calibration of Mu r_s might have contributed in the increased efficiency of the scenarios that employ those parameters, especially as 11 towers that were used in the current study overlap with those in the Mu et al. (2011) study.

474 **The top-ranked model and parameterizations**: Overall, the top-ranked scenarios (see Table 2) for
475 each biome were: PM^3 for grasslands (0.53) and shrublands (0.35), Mu^1 for croplands (0.67), SW^3 for
476 evergreen needleleaf forest (0.38) and SW^4 for deciduous broadleaf forest sites (0.76) (NSE_{avg} shown
477 in parenthesis). These results highlight the role of model structure in evaporation modelling, as the
478 single source PM model provided better results over short canopies (grasslands and shrublands) and
479 the two-layer structure of the SW model provided better results over forest biomes. Interestingly,
480 the three-source Mu model structure provided an exception here, as it performed the best when
481 applied over croplands (which have relatively short canopies).

482 The common element of the top-ranked scenarios is the use of the Mu surface resistance. Likewise,
483 PM^3, SW^3 and Mu^1 all use the Thom aerodynamic resistance with dynamic roughness, while SW^4
484 uses the Mu r_a. The Mu model itself showed low sensitivity to r_a parameterization, while its r_s
485 parameterization improved other models.

486 **Comparison with alternative process-based evaporation models:** The Penman-Monteith model
487 variants of the current study showed variable performances in evaporation estimation across the
488 different studied biomes, even when considering the top-ranked configurations. In comparison, a
489 number of alternative process-based models have shown superior performance in related studies.
490 Recently, Ershadi et al. (2014) compared four process-based evaporation models that included the
491 Surface Energy Balance System (SEBS) (Su, 2002), PT-JPL (Fisher et al., 2008), Advection-Aridity
492 (Brutsaert and Stricker, 1979) and a single-source PM model with Jarvis r_s and Thom r_a with dynamic
493 roughness (i.e. similar to PM^2). Using the same dataset of the current study, they found that an
494 ensemble of model responses had the best performance, followed by the PT-JPL and SEBS. The issue
495 of appropriate model selection is obviously a key consideration that will ultimately be guided by user
496 experience, data needs and data availability. Nevertheless, adopting a multi-model strategy for flux
497 estimation seems a useful approach in understanding and constraining the uncertainties that
498 emerge from model structure and parameterization configurations.

4.2 Issues of Data Uncertainty

As discussed above, a consideration in the choice of both the model and parameterization scheme is the availability of reliable data. Application of the surface resistance method of the Mu model is important in relaxing the need for soil moisture data and is likely to facilitate its application in evaporation estimation from field to larger scales (Mu et al., 2012). Similar results were found in previous work using a modified Priestly-Taylor model (PT-JPL model; Fisher et al., 2008). Like the Mu model, the PT-JPL approach does not require wind speed or soil moisture data, and recent comparisons against more complex models illustrated that the PT-JPL performs well (Vinukollu et al., 2011; Ershadi et al., 2014).

The aerodynamic resistance scheme used by the top-ranked scenarios examined here (except for deciduous broadleaf forest sites) were all based on Thom r_a with dynamic roughness, which requires reliable wind speed and canopy height data. Generally, accurate in-situ based wind speed data are not routinely available for many study sites. Likewise, the only source for canopy height at the global scale is a static product developed by NASA-JPL (Simard et al., 2011), which has limited capability over short vegetation (e.g. grasslands and croplands). Although the Mu model is designed for large scale applications with coarse spatial (1 km) and temporal (8 day to yearly) resolutions, the results of the current study show that in the absence of required forcing data the Mu resistance scheme could be used at the tower scale with reasonable performance.

Part of the deficiencies in model performance, especially over shrubland sites (NSE_{avg} < 0.34) is likely related to the spatio-temporal resolution (i.e. 250 m, 16 days) of the MODIS data. MODIS data are used in the estimation of vegetation indices, which are subsequently used for parameterization of aerodynamic and surface resistances. Shrubland sites display considerable land surface heterogeneity and the contrasting bare soil and vegetation elements may not be well captured at the coarse remote sensing pixels (Stott et al., 1998; Montandon and Small, 2008). A difference between the results of this and previous studies that have reported higher performance of PM type

models, may reflect the inherent uncertainties introduced via the input data, since the majority of prior investigations were performed with detailed field observations of vegetation characteristics (Huntingford et al., 1995; Li et al., 2011). Clearly there is a need for high-quality in-situ phenological descriptions to undertake the types of globally distributed analysis performed here, but unfortunately they are often lacking. Likewise, a better understanding of the inherent scale issues in flux estimation is required, particularly for the impact of both spatial and temporal scaling on the performance of aerodynamic and surface resistance terms (McCabe and Wood, 2006; Ershadi et al., 2013).

5 Conclusion

The influence of model structure and resistance parameterization is an important, but often overlooked, consideration in the performance of Penman-Monteith type evaporation models. Understanding the effects of model structure and parameterization configurations is non-trivial due to the mixed influence of data uncertainty, hydrometeorological variability and the complexity of the modelling system (Raupach and Finnigan, 1988). In this study, the effects of model structure and choice of resistance parameterization were investigated using three Penman-Monteith type models. The structure of the models varied from single-source, to two-layer and three-source. To examine the influence of model parameterization, a number of commonly used resistance schemes were substituted into the models, with flux estimates evaluated against locally measured evaporation at a number of eddy-covariance tower sites.

Results illustrated the considerable variability in model performance over the different biomes, with no single model structure or scenario providing a consistently top-ranked result over the twenty study sites. Indeed, the top-ranked scenarios highlighted the importance of model structure. Except over croplands, where the three-source Mu model structure performed the best, the single-source PM structure performed better over short canopies while the two-layer SW structure performed

548 better over forest canopies. Changes in resistance parameterizations, in particular the surface
549 resistance, were also seen to strongly influence the performance of the models.

550 A key consideration from the findings of this work relates to the application of Penman-Monteith
551 type models across a range of hydrological and related disciplines. Penman-Monteith type
552 approaches have been used with modifications in structure and parameterizations in a number of
553 global scale datasets (Zhang et al., 2010), global circulation models (Dolman, 1993) and land surface
554 model applications. Hence, uncertainties and errors originating from non-optimum structure or
555 parameterization of the models can significantly influence the accuracy of simulation results,
556 evaluation of global trends (Jiménez et al., 2011; Mueller et al., 2013) and decisions based on such
557 results, including but not limited to drought (Sheffield and Wood, 2008), land-atmosphere
558 interactions (Seneviratne et al., 2006) and climate change projections (Droogers et al., 2012).

559 As the focus of this paper was on reporting biome-level efficiency of model and parameterization
560 configurations, the influence of vegetation phenology (e.g. LAI, fractional vegetation cover), land
561 cover and climate zone were not explicitly considered in the analysis. Future work is needed to focus
562 on site-level evaluation of the models to address these important issues. Furthermore, given that
563 the top-ranked scenarios identified in this study varied across different biomes, an ensemble model
564 based assessment might be an appropriate approach for global flux estimation (Jiménez et al., 2011;
565 Mueller et al., 2011; Mueller et al., 2013). Alternatively, a biome-specific tiled evaporation product
566 could also be developed by using the best model and parameterization configuration for each biome
567 type. In either case, further understanding the role of parameterization on model performance is
568 critical in assessing the impact of choice on derived products.

569 ## Acknowledgement

570 Funding for this research was provided via an Australian Research Council (ARC) Linkage (LP0989441)
571 and Discovery (DP120104718) project, together with a top-up scholarship to support Dr Ali Ershadi

572 from the National Centre for Groundwater Research and Training (NCGRT) in Australia during his
573 PhD. Research reported in this publication was also supported by the King Abdullah University of
574 Science and Technology (KAUST). We thank the FLUXNET site investigators for allowing the use of
575 their meteorological data. This work used eddy-covariance data acquired by the FLUXNET
576 community and in particular by the AmeriFlux (U.S. Department of Energy, Biological and
577 Environmental Research, Terrestrial Carbon Program: DE-FG02-04ER63917 and DE-FG02-04ER63911)
578 and OzFlux programs. We acknowledge the financial support to the eddy-covariance data
579 harmonization provided by CarboEuropeIP, FAO-GTOS-TCO, iLEAPS, Max Planck Institute for
580 Biogeochemistry, National Science Foundation, University of Tuscia, Université Laval and
581 Environment Canada and US Department of Energy and the database development and technical
582 support from Berkeley Water Centre, Lawrence Berkeley National Laboratory, Microsoft Research
583 eScience, Oak Ridge National Laboratory, University of California - Berkeley, University of Virginia.
584 Data supplied by T. Kolb, School of Forestry, Northern Arizona University, for the US-Fuf site was
585 supported by grants from the North American Carbon Program/USDA NRI (2004-35111-15057; 2008-
586 35101-19076), Science Foundation Arizona (CAA 0-203-08), and the Arizona Water Institute. Matlab
587 scripts for automatic extraction of NDVI time series at towers were provided by Dr Tristan Quaife,
588 University College London via the web portal at http://daac.ornl.gov/MODIS/MODIS-
589 menu/modis_webservice.html

590

Appendix A: Details of the Selected Eddy-Covariance Towers

Table A1: Selected eddy-covariance towers and their characteristics (Ershadi et al., 2014). z_g is the site elevation (above sea level) in m, z_m is tower height in m, h_c is the canopy height in m, Y is the number of years of data and L is the processing level of data. Abbreviations for climate types are defined for Sub-Tropical Mediterranean (STM), Temperate Continental (TC), Temperate (TEM) and Tropical (TRO).

	ID	Name	Country	Climate	Lat.	Lon.	z_g	z_m	h_c	Y	L	Reference
		Grasslands										
G1	PT-Mi2	Mitra IV Tojal	Portugal	STM	38.5	-8.0	190	2.5	0.05	2	3	(Gilmanov et al., 2007)
G2	US-Aud	Audubon Research Ranch	USA	Dry	31.6	-110.5	1469	4	0.15	4	3	(Krishnan et al., 2012)
G3	US-Goo	Goodwin Creek	USA	STM	34.3	-89.9	87	4	0.3	4	3	(Hollinger et al., 2010)
G4	US-Fpe	Fort Peck	USA	Dry	48.3	-105.1	634	3.5	0.3	4	3	(Horn and Schulz, 2011)
		Croplands										
C1	US-ARM	ARM SGP – Lamont	USA	STM	36.6	-97.5	314	60	0.5	4	3	(Lokupitiya et al., 2009)
C2	US-Ne3	Mead – rainfed	USA	TC	41.2	-96.4	363	6	2.5	10	3	(Richardson et al., 2006)
C3	US-Ne1	Mead – irrigated	USA	TC	41.2	-96.5	361	6	3	10	3	(Richardson et al., 2006)
C4	US-Bo1	Bondville	USA	TC	40.0	-88.3	219	10	3	7	3	(Hollinger et al., 2010)
		Shrubland/Woody Savannah										
S1	US-SRc	Santa Rita Creosote	USA	Dry	31.9	-110.8	991	4.25	1.7	1.5	2	(Cavanaugh et al., 2011)
S2	US-SRM	Santa Rita Mesquite	USA	Dry	31.8	-110.9	1116	6.4	2.5	7	2	(Scott et al., 2009)
S3	BW-Ma1	Maun- Mopane Woodland	Botswana	Dry	-19.9	23.6	950	13.5	8	2	3	(Veenendaal et al., 2004)
S4	AU-How	Howard Springs	Australia	TRO	-12.5	131.2	38	23	15	5	3	(Hutley et al., 2005)
		Evergreen Needleleaf Forest										
E1	NL-Loo	Loobos	Netherlands	TEM	52.2	5.7	25	52	15.9	5	3	(Sulkava et al., 2011)
E2	US-Fuf	Flagstaff - Unmanaged Forest	USA	TC	35.1	-111.8	2180	23	18	6	2	(Román et al., 2009)
E3	DE-Tha	Anchor St. Tharandt - old spruce	Germany	TEM	51.0	13.6	380	42	30	2	3	(Delpierre et al., 2009)
E4	US-Wrc	Wind River Crane Site	USA	TEM	45.8	-122.0	371	85	56.3	9	2	(Wharton et al., 2009)
		Deciduous Broadleaf Forest										
D1	US-MOz	Missouri Ozark Site	USA	STM	38.7	-92.2	219	30	24.2	5	2	(Hollinger et al., 2010)
D2	US-WCr	Willow Creek	USA	TC	45.8	-90.1	520	30	24.3	5	3	(Curtis et al., 2002)
D3	US-MMS	Morgan Monroe State Forest	USA	STM	39.3	-86.4	275	48	27	6	2	(Dragoni et al., 2011)
D4	DE-Hai	Hainich	Germany	TEM	51.1	10.5	430	43.5	33	3	3	(Rebmann et al., 2005)

Appendix B: Jarvis Surface Resistance Parameterization Method

The Jarvis method for estimation of surface resistance (r_s) can be expressed as:

$$r_s = \frac{r_s^{min}}{LAI \times F_1 \times F_2 \times F_3 \times F_4} \quad \text{B1}$$

Where r_s^{min} is the minimum canopy resistance (s.m^{-1}), LAI is the leaf area index (m^2.m^{-2}) and F_1, F_2, F_3 and F_4 are weighting functions representing the effects of solar radiation, humidity, soil moisture and air temperature on plant stress. Following Chen and Dudhia (2001), the weighting functions for Jarvis method type surface resistance are defined as following:

$$F_1 = \frac{r_s^{min}/r_s^{max}+f}{1+f} \text{ with } f = 0.55\frac{R_g}{R_{gl}}\left(\frac{2}{LAI}\right)$$

$$F_2 = \frac{1}{1+h_s(q^* - q)} \quad \text{B2}$$

$$F_3 = 1 - 0.0016\left(T_{ref} - T_a\right)^2$$

$$F_4 = \sum_{i=1}^{N_{root}} \frac{(\theta_i - \theta_{wilt})d_i}{(\theta_{ref} - \theta_{wilt})d_t}$$

where r_s^{max} is the maximum canopy resistance (s.m^{-1}), R_{gl} is the minimum solar radiation necessary for transpiration (W.m^{-2}), R_g is the incident solar radiation (W.m^{-2}), h_s is a parameter associated with the water vapor deficit, $q^* - q$ represents the water vapour deficit (kg.kg^{-1}), q^* is saturation specific humidity, q is actual specific humidity, T_{ref} is the optimal temperature for photosynthesis (K) and T_a is the air temperature (K). d_i is the thickness of the ith soil layer (m), d_t is the total thickness of the soil layer (m) and N_{root} is the number of soil layers. In this study, the observation depth of the soil moisture sensor(s) (5 to 10 cm) is considered to be representative of the overall soil column. Obviously, there is potential for rapid changes in the observed near-surface soil moisture (as a response to precipitation) which may not accurately reflect the deeper soil column response, especially for sites with deeply rooted system. However, as there is limited

613 availability of soil moisture data with which to refine the technique, we employ this relatively simple
614 scheme as a compromise. The G1, S3, S4, E1, E3 and D4 towers (see Table A1) had one soil layer,
615 and the rest of towers had two soil layers included in the analysis. Values of r_s^{min}, r_s^{max}, R_{gl}, h_s and
616 T_{ref} were based on the vegetation lookup tables used in the NOAH land surface model (see Kumar
617 et al., 2011).

618 Soil moisture content thresholds for field capacity (θ_{ref}) and wilting point (θ_{wilt}) provide
619 characteristics of the soil type. As soil type information is not available for all sites from field
620 investigations and the values in existing global soil databases are not reliable at the point scale, long-
621 term surface layer soil moisture observations from each tower are used to determine soil moisture
622 thresholds (Calvet et al., 1998; Zotarelli et al., 2010). To do this, the field capacity is determined as
623 the 99th percentile of the "after rain" soil moisture records of the tower. The estimated θ_{ref} is
624 constrained by the maximum value of θ_{ref} in the NOAH soil table, as the length of soil moisture data
625 might not be sufficient to result a realistic θ_{ref}. Similarly, the wilting point threshold is determined
626 from the 1st percentile of the soil moisture records, but capped to the minimum value of θ_{wilt} in the
627 NOAH soil table. Both vegetation and soil parameter tables of the NOAH model can be obtained
628 from http://www.ral.ucar.edu/research/land/technology/lsm.php.

629

Appendix C: Shuttleworth-Wallace Model

In the SW model, C_c and C_s are resistance functions for canopy and soil (respectively) and are given by the following equations:

$$C_c = \left[1 + \frac{R_c R_a}{R_s(R_c + R_a)}\right]^{-1} \quad \text{C1}$$

$$C_s = \left[1 + \frac{R_s R_a}{R_c(R_s + R_a)}\right]^{-1} \quad \text{C2}$$

where

$$R_a = (\Delta + \gamma) r_a^a \quad \text{C3}$$

The bulk stomatal resistance of the canopy (r_s^c) is a surface resistance, which is influenced by the surface area of the vegetation. In the original derivation of the SW model, the bulk stomatal resistance was calculated by upscaling the leaf scale stomatal resistance (r_{ST}) based on the leaf area index (LAI) as $r_s^c = r_{ST}/2 \times LAI$, with r_{ST} assumed as a constant value or calibrated based on evaporation observations. However, we derive the bulk canopy resistance using the Jarvis method of Noilhan and Planton (1989) (see Appendix B), as is used in a number of previous studies of the Shuttleworth-Wallace model (e.g. Zhou et al., 2006; Irmak, 2011). The soil surface resistance (r_s^s) is derived from the above mentioned Jarvis method, using the "Barren and Sparsely Vegetated" category of the NOAH vegetation table for the bare soil.

Three aerodynamic resistances appear in the SW model: an aerodynamic resistance between the soil/substrate surface and the canopy source height (r_a^s), a bulk boundary layer resistance of vegetative elements in the canopy (r_a^c), and an aerodynamic resistance between the canopy source height and a reference level above the canopy (r_a^a). The bulk boundary layer resistance (r_a^c) is calculated by scaling the leaf scale mean boundary layer resistance r_b to the canopy scale using LAI, as $r_a^c = r_b/2 \times LAI$, with r_b considered constant at 25 s·m^{-1} (Shuttleworth and Wallace, 1985).

650 However, r_a^a and r_a^s are calculated using the following equations (Shuttleworth and Gurney, 1990)

651 (i.e. SG90):

$$r_a^a = \frac{1}{\kappa u_*}\ln\left(\frac{z-d_0}{h_c-d_0}\right) + \frac{h_c}{nK_h}\left\{\exp\left[n\left(1-\frac{z_{0m}+d_0}{h_c}\right)\right]-1\right\} \quad \text{C4}$$

$$r_a^s = \frac{h_c\exp(n)}{nK_h}\left\{\exp\left(-\frac{nz'_{0m}}{h_c}\right) - \exp\left[-n\left(\frac{z_{0m}+d_0}{h_c}\right)\right]\right\} \quad \text{C5}$$

652 where z'_{0m} is the roughness length of bare soil surface (=0.01 m) (van Bavel and Hillel, 1976)

653 and n is the eddy diffusivity decay constant (dimensionless), which is assumed fixed at 2.5 for

654 agricultural crops by Shuttleworth and Wallace (1985). However, following Zhang et al. (2008) and

655 based on the values given by Brutsaert (1982), we assume $n = 2.5$ when $h_c < 1$ m and $n = 4.25$

656 when $h_c > 10$ m. For the cases where $1 \geq h_c \geq 10$, a linear interpolation is applied as $n =$

657 $0.1944h_c + 2.3056$. The eddy diffusion coefficient at the top of canopy (K_h in $m^2 \cdot s^{-1}$) is calculated as

658 $K_h = \kappa u_*(h_c - d_0)$, with the friction velocity (u_* in $m.s^{-1}$) calculated as $u_* = \kappa u_a / \ln[(z-d_0)/$

659 $z_{0m}]$. As is common in general applications of the SW model, the roughness variables d_0 and z_{0m}

660 are assumed as a fraction of the canopy height (Brutsaert, 2005), as in Equation 3.

661

Appendix D: Mu Model Evaporation Component and Resistances

D1. Evaporation from Wet Canopy

Evaporation from a wet canopy (i.e. intercepted water) is calculated using the following equation:

$$\lambda E_{wc} = f_w \frac{\Delta A_c + f_c \rho c_p (e^* - e)/r_a^{wc}}{\Delta + \gamma \frac{r_s^{wc}}{r_a^{wc}}} \quad \text{D1}$$

where f_c is fractional vegetation cover. f_w is the relative surface wetness and calculated as $f_w = RH^4$, which is based on the concept originally developed by Fisher et al. (2008). In the original Mu model, daily average values of RH were used and f_w was assumed zero when daily average $RH < 0.7$. However, here we used hourly (or half-hourly) data and did not filter f_w based on low RH values.

The aerodynamic resistance r_a^{wc} and surface resistance r_s^{wc} for wet canopy are defined as:

$$r_a^{wc} = \frac{r_h^{wc} r_r^{wc}}{r_h^{wc} + r_r^{wc}} \quad \text{D2}$$

$$r_s^{wc} = \frac{1}{f_w g_e LAI} \quad \text{D3}$$

where r_h^{wc} is wet canopy resistance to sensible heat transfer and r_r^{wc} is the wet canopy resistance to radiative heat transfer, which are formulated as following:

$$r_h^{wc} = \frac{1}{f_w g_h LAI}$$

$$r_r^{wc} = \frac{\rho c_p}{4\sigma T_a^3} \quad \text{D4}$$

g_e and g_h are leaf conductance to evaporated water vapor and sensible heat (respectively) per unit LAI, T_a is air temperature (°C) and σ is the Stefan-Boltzmann constant. Based on Mu et al. (2011), g_e and g_h are assumed similar and constant for each biome as listed in Table B1. The available energy

for crop and soil is partitioned based on the fractional vegetation cover (f_c) as $A_s = f_c R_n$ and $A_s = (1 - f_c)R_n - G_0$.

D2. Canopy Transpiration

The canopy transpiration λE_t is calculated as:

$$\lambda E_t = (1 - f_w)\frac{\Delta A_c + f_c \rho c_p (e^* - e)/r_a^t}{\Delta + \gamma\left(1 + \frac{r_s^t}{r_a^t}\right)} \quad \text{D5}$$

Where r_a^t and r_s^t are aerodynamic and surface resistances for transpiration, respectively. The bulk canopy resistance (r_s^t) is the inverse of the bulk canopy conductance (C_c) and calculated as:

$$r_s^t = \frac{1}{C_c} \quad \text{D6}$$

The assumption here is that the stomatal conductance (G_s^{st}) and cuticular conductance (G_s^{cu}) are in parallel, but both are in series with the canopy boundary-layer conductance G_s^b. Therefore, the canopy conductance to transpiration is calculated as:

$$C_c = \begin{cases} (1 - f_w)\dfrac{(G_s^{st} + G_s^{cu})G_s^b}{G_s^{st} + G_s^{cu} + G_s^b} LAI & , LAI > 0, (1 - f_w) > 0 \\ 0 & , LAI = 0, (1 - f_w) = 0 \end{cases} \quad \text{D7}$$

Where $G_s^b = g_h$, $G_s^{cu} = r_{corr} g_{cu}$ and $G_s^{st} = c_L m(T_{min}) m(VPD) r_{corr}$ with VPD being the vapor pressure deficit (Pa). The leaf cuticular conductance (g_{cu}) is per unit LAI, and assumed equal to 0.00001 m.s^{-1} for all biomes. Also, the mean potential stomatal conductance (c_L) is per unit leaf area, and is assumed constant for each biome (Table B1). The r_{corr} is the correction factor for G_s^{st} to adjust it based on the standard air temperature and pressure (20 °C and 101,300 Pa) using the following equation:

$$r_{corr} = \frac{1}{\frac{101300}{Pa}\left(\frac{T_a + 273.15}{293.15}\right)^{1.75}} \quad \text{D8}$$

691 $m(T_{min})$ is a multiplier that limits potential stomatal conductance by minimum air temperature
692 (T_{min}), and $m(VPD)$ is a multiplier used to reduce the potential stomatal conductance when
693 $VPD = e^* - e$ is high enough to reduce canopy conductance. Following Mu et al. (2007), $m(T_{min})$
694 and $m(VPD)$ are calculated as following:

$$m(T_{min}) = \begin{cases} 1 & T_{min} \geq T_{min}^{open} \\ \dfrac{T_{min} - T_{min}^{close}}{T_{min}^{open} - T_{min}^{close}} & T_{min}^{close} < T_{min} < T_{min}^{open} \\ 0 & T_{min} \leq T_{min}^{close} \end{cases} \quad \text{D9}$$

$$m(VPD) = \begin{cases} 1 & VPD \leq VPD_{open} \\ \dfrac{VPD_{close} - VPD}{VPD_{close} - VPD_{open}} & VPD_{open} < VPD < VPD_{open} \\ 0 & VPD \geq VPD_{close} \end{cases} \quad \text{D10}$$

695 Values of T_{min}^{open}, T_{min}^{close}, VPD_{open} and VPD_{close} are listed in Table B1 for each biome type. Also, the
696 aerodynamic resistance to canopy transpiration, r_a^t, is calculated based on the convective heat
697 transfer resistance r_h and radiative heat transfer resistance r_r, assuming they are in parallel using
698 the following equation (Thornton, 1998):

$$r_a^t = \frac{r_h^t r_r^t}{r_h^t + r_r^t} \quad \text{D11}$$

699 Where $r_h^t = 1/g_{bl}$ and $r_r^t = r_r^{wc}$ with g_{bl} being the leaf-scale boundary layer conductance
700 per unit *LAI* and assumed equal to that of the sensible heat (i.e. $g_{bl} = g_h$).

701 D3. Soil Evaporation

702 Evaporation from the soil surface is calculated as the sum of evaporation from wet soil (λE_{ws}) and
703 evaporation from saturated soil (λE_{ss}), such that:

$$\lambda E_s = \lambda E_{ws} + \lambda E_{ss}. \quad \text{D12}$$

704 Partitioning of the soil surface to wet and saturated components is based on the relative surface
705 wetness f_w, with the evaporation from the wet soil calculated as:

$$\lambda E_{ws} = f_w \frac{\Delta A_s + (1 - f_c)\rho c_p (e^* - e)/r_a^s}{\Delta + \gamma \frac{r_s^s}{r_a^s}}. \quad \textbf{D13}$$

706 Similarly, evaporation from the saturated soil is calculated as:

$$\lambda E_{ss} = RH^{VPD/\beta}(1 - f_w)\frac{\Delta A_s + (1 - f_c)\rho c_p (e^* - e)/r_a^s}{\Delta + \gamma \frac{r_s^s}{r_a^s}}$$

707 where r_a^s and r_s^s are aerodynamic and surface resistances for the soil surface. $RH^{VPD/\beta}$ is a
708 soil moisture constraint that is used following Fisher et al. (2008). This function is based on the
709 complementary hypothesis and describes land-atmosphere interactions via the air vapour pressure
710 deficit *VPD* and relative humidity *RH*, with β assigned a constant value of 200. The soil surface
711 resistance r_s^s is calculated as:

$$r_s^s = r_{corr} r_{totc} \quad \textbf{D14}$$

712 where r_{totc} is a function of *VDP* and biological parameters r_{bl}^{min} and r_{bl}^{max} as follows:

$$r_{totc} = \begin{cases} r_{bl}^{max} & VPD \le VPD_{open} \\ r_{bl}^{max} - \dfrac{\left(r_{bl}^{max} - r_{bl}^{min}\right) \times (VPD_{close} - VPD)}{VPD_{close} - VPD_{open}} & VPD_{open} < VPD < VPD_{close} \\ r_{bl}^{min} & VPD \ge VPD_{close} \end{cases} \quad \textbf{D15}$$

713 VPD_{open} is the *VPD* when there is no water stress on transpiration and VPD_{close} is the *VPD* when
714 water stress causes stomata to close almost completely, halting plant transpiration. Values for r_{bl}^{max},
715 r_{bl}^{min}, VPD_{open} and VPD_{close} are listed in Table B1.

716 The aerodynamic resistance at the soil surface (r_a^s) is parallel to both the resistance to convective
717 heat transfer (r_h^s) and the resistance to radiative heat transfer r_r^s, with its components calculated as:

$$r_a^s = \frac{r_h^s r_r^s}{r_h^s + r_r^s} \quad \textbf{D16}$$

718 Where $r_r^s = r_r^{wc}$ and $r_h^s = r_s^s$.

Table 2 shows the Biome-Property-Lookup-Table (BPLT) used in the Mu model. As explained by Mu et al. (2011), VPD and T_{min} parameters were derived from calibrations performed by Zhao et al. (2005), but other parameters were calibrated based on biome aggregated observed evaporation and Gross Primary Production (GPP) values at 46 AmeriFlux tower sites, some of which are included in the current study.

Table B1: The Biome-Property-Lookup-Table (BPLT) adopted from Mu et al. (2011). Land covers are defined as evergreen needleleaf forest (ENF), evergreen broadleaf forest (EBF), deciduous needleleaf forest (DNF), deciduous broadleaf forest (DBF), mixed forest (MF), woody savannahs (WL), savannahs (SV), closed shrubland (CSH), open shrubland (OSH) and cropland (CRO). GRA class is for grassland, urban and built-up, and barren or sparsely vegetated biomes, collectively.

Crop	ENF	EBF	DNF	DBF	MF	CSH	OSH	WL	SV	GRA	CRO
T_{min}^{open} (°C)	8.31	9.09	10.44	9.94	9.5	8.61	8.8	11.39	11.39	12.02	12.02
T_{min}^{close} (°C)	-8	-8	-8	-6	-7	-8	-8	-8	-8	-8	-8
VPD_{close} (Pa)	3000	4000	3500	2900	2900	4300	4400	3500	3600	4200	4500
VPD_{open} (Pa)	650	1000	650	650	650	650	650	650	650	650	650
g_h ($m.s^{-1}$)	0.04	0.01	0.04	0.01	0.04	0.04	0.04	0.08	0.08	0.02	0.02
g_e ($m.s^{-1}$)	0.04	0.01	0.04	0.01	0.04	0.04	0.04	0.08	0.08	0.02	0.02
c_L ($m.s^{-1}$)	0.0032	0.0025	0.0032	0.0028	0.0025	0.0065	0.0065	0.0065	0.0065	0.007	0.007
r_{bl}^{min} ($m.s^{-1}$)	65	70	65	65	65	20	20	25	25	20	20
r_{bl}^{max} ($m.s^{-1}$)	95	100	95	100	95	55	55	45	45	50	50

Appendix E: The Dynamic Roughness Parameterization Method

In the Su et al. (2001) method, the roughness height for momentum transfer is calculated as:

$$z_{0m} = h_c\left(1 - \frac{d_0}{h_c}\right)\exp\left(-\frac{\kappa}{\eta}\right) \quad \text{E1}$$

where h_c is the canopy height and η is the ratio of friction velocity to the wind speed at the canopy top, calculated as $\eta = c_1 - c_2\exp(-c_3 C_d LAI)$ with $c_1 = 0.32$, $c_2 = 0.264$, $c_3 = 15.1$ and the drag coefficient $C_d = 0.2$. The roughness length for heat transfer (z_{0h}) can be derived by assuming an exponential relationship between z_{0m} and z_{0h} as $z_{0h} = z_{0m}/\exp(\kappa B^{-1})$, where B^{-1} is the inverse Stanton number. To estimate the κB^{-1} parameter, the method of Su et al. (2001) suggests:

$$\kappa B^{-1} = \frac{\kappa C_d}{4C_t\beta\left(1 - \exp\left(-\frac{n_{ec}}{2}\right)\right)} f_c^2 + 2f_c f_s \frac{\kappa\eta z_{0m}/h_c}{C_t^*} + \kappa B_s^{-1} f_s^2 \quad \text{E2}$$

where f_c is the fractional canopy coverage and f_s is its complement (for soil coverage). C_t is the heat transfer coefficient of the leaf, C_t^* is the heat transfer coefficient of the soil and n_{ec} is within-canopy wind speed profile extinction coefficient.

As noted by Su (2002), the first term of equation E2 follows the full canopy model of Choudhury and Monteith (1988), the third term is that of Brutsaert (1982) for a bare soil surface and the second term describes the interaction between vegetation and a bare soil surface. Following Brutsaert (1999), for a bare soil surface the κB_s^{-1} is calculated as $\kappa B_s^{-1} = 2.46 Re_*^{1/4} - \ln(7.4)$ with Re_* being the Reynolds number. More details about the methodology and formulation are available in Su et al. (2001) and Su (2002).

751 # References

752 Allen, R.G., Pereira, L.S., Howell, T.A., Jensen, M.E., 2011. Evapotranspiration information reporting:
753 II. Recommended documentation. Agricultural Water Management, 98(6): 921-929.

754 Bailey, W.G., Davies, J.A., 1981. The effect of uncertainty in aerodynamic resistance on evaporation
755 estimates from the combination model. Boundary-Layer Meteorology, 20(2): 187-199.

756 Baldocchi, D. et al., 2001. FLUXNET: A New Tool to Study the Temporal and Spatial Variability of
757 Ecosystem–Scale Carbon Dioxide, Water Vapor, and Energy Flux Densities. Bulletin of the
758 American Meteorological Society, 82(11): 2415-2434.

759 Brutsaert, W., 1982. Evaporation Into the Atmosphere : theory, history, and applications. Reidel
760 Publishing, Dordrecht etc., 299 pp.

761 Brutsaert, W., 1999. Aspects of Bulk Atmospheric Boundary Layer Similarity Under Free-Convective
762 Conditions. Rev. Geophys., 37.

763 Brutsaert, W., 2005. Hydrology : An Introduction. Cambridge University Press, Cambridge, 605 pp.

764 Brutsaert, W., Stricker, H., 1979. An advection-aridity approach to estimate actual regional
765 evapotranspiration. Water Resour. Res., 15(2): 443-450.

766 Calvet, J.C., Noilhan, J., Bessemoulin, P., 1998. Retrieving the root-zone soil moisture from surface
767 soil moisture or temperature estimates: A feasibility study based on field measurements.
768 Journal of Applied Meteorology, 37(4): 371-386.

769 Cavanaugh, M.L., Kurc, S.A., Scott, R.L., 2011. Evapotranspiration partitioning in semiarid shrubland
770 ecosystems: a two-site evaluation of soil moisture control on transpiration. Ecohydrology,
771 4(5): 671-681.

772 Chen, F., Dudhia, J., 2001. Coupling an Advanced Land Surface–Hydrology Model with the Penn
773 State–NCAR MM5 Modeling System. Part I: Model Implementation and Sensitivity. Monthly
774 Weather Review, 129(4): 569-585.

775 Choudhury, B.J., Monteith, J.L., 1988. A four-layer model for the heat budget of homogeneous land
776 surfaces. Q. J. R. Meteorol. Soc., 114(480): 373-398.

777 Curtis, P.S. et al., 2002. Biometric and eddy-covariance based estimates of annual carbon storage in
778 five eastern North American deciduous forests. Agricultural and Forest Meteorology, 113(1):
779 3-19.

780 Delpierre, N. et al., 2009. Exceptional carbon uptake in European forests during the warm spring of
781 2007: a data–model analysis. Global Change Biology, 15(6): 1455-1474.

782 Dolman, A.J., 1993. A multiple-source land surface energy balance model for use in general
783 circulation models. Agricultural and Forest Meteorology, 65(1–2): 21-45.

784 Dragoni, D. et al., 2011. Evidence of increased net ecosystem productivity associated with a longer
785 vegetated season in a deciduous forest in south-central Indiana, USA. Global Change Biology,
786 17(2): 886-897.

787 Droogers, P. et al., 2012. Water resources trends in Middle East and North Africa towards 2050.
788 Hydrol. Earth Syst. Sci., 16(9): 3101-3114.

789 Ershadi, A., McCabe, M.F., Evans, J.P., Chaney, N.W., Wood, E.F., 2014. Multi-site evaluation of
790 terrestrial evaporation models using FLUXNET data. Agricultural and Forest Meteorology,
791 187(0): 46-61.

792 Ershadi, A., McCabe, M.F., Evans, J.P., Walker, J.P., 2013. Effects of spatial aggregation on the multi-
793 scale estimation of evapotranspiration. Remote Sensing of Environment, 131: 51-62.

794 Ferguson, C.R., Sheffield, J., Wood, E.F., Gao, H., 2010. Quantifying uncertainty in a remote sensing-
795 based estimate of evapotranspiration over continental USA. International Journal of Remote
796 Sensing, 31(14): 3821-3865.

797 Finnigan, J.J., Clement, R., Malhi, Y., Leuning, R., Cleugh, H.A., 2003. A re-evaluation of long-term flux
798 measurement techniques - Part I: Averaging and coordinate rotation. Boundary-Layer
799 Meteorology, 107(1): 1-48.

800 Fisher, J.B., DeBiase, T.A., Qi, Y., Xu, M., Goldstein, A.H., 2005. Evapotranspiration models compared
801 on a Sierra Nevada forest ecosystem. Environmental Modelling & Software, 20(6): 783-796.

802 Fisher, J.B., Tu, K.P., Baldocchi, D.D., 2008. Global estimates of the land-atmosphere water flux based
803 on monthly AVHRR and ISLSCP-II data, validated at 16 FLUXNET sites. Remote Sensing of
804 Environment, 112(3): 901-919.

805 Foken, T., Leuning, R., Oncley, S.R., Mauder, M., Aubinet, M., 2012. Corrections and Data Quality
806 Control. In: Aubinet, M., Vesala, T., Papale, D. (Eds.), Eddy Covariance, A Practical Guide to
807 Measurement and Data Analysis. Springer.

808 Gilmanov, T.G. et al., 2007. Partitioning European grassland net ecosystem CO2 exchange into gross
809 primary productivity and ecosystem respiration using light response function analysis.
810 Agriculture, ecosystems & environment, 121(1): 93-120.

811 Hollinger, D.Y. et al., 2010. Albedo estimates for land surface models and support for a new
812 paradigm based on foliage nitrogen concentration. Global Change Biology, 16(2): 696-710.

813 Horn, J.E., Schulz, K., 2011. Identification of a general light use efficiency model for gross primary
814 production. Biogeosciences, 8: 999 - 1021.

815 Huntingford, C., Allen, S.J., Harding, R.J., 1995. An intercomparison of single and dual-source
816 vegetation-atmosphere transfer models applied to transpiration from sahelian savannah.
817 Boundary-Layer Meteorology, 74(4): 397-418.

818 Hutley, L.B., Leuning, R., Beringer, J., Cleugh, H.A., 2005. The utility of the eddy covariance
819 techniques as a tool in carbon accounting: tropical savanna as a case study. Australian
820 Journal of Botany, 53(7): 663-675.

821 Inclán, M.G., Forkel, R., 1995. Comparison of energy fluxes calculated with the Penman-Monteith
822 equation and the vegetation models SiB and Cupid. Journal of Hydrology, 166(3-4): 193-211.

823 Irmak, A., 2011. Evapotranspiration - Remote Sensing and Modeling. InTech, Croatia.

824 Irmak, S., Mutiibwa, D., 2010. On the dynamics of canopy resistance: Generalized linear estimation
825 and relationships with primary micrometeorological variables. Water Resour. Res., 46(8):
826 W08526.

827 Jacquemin, B., Noilhan, J., 1990. Sensitivity study and validation of a land surface parameterization
828 using the HAPEX-MOBILHY data set. Boundary-Layer Meteorology, 52(1): 93-134.

829 Jiménez-Muñoz, J. et al., 2009. Comparison between fractional vegetation cover retrievals from
830 vegetation indices and spectral mixture analysis: Case Study of PROBA/CHRIS data dver an
831 agricultural area. Sensors, 9(2): 768-793.

832 Jiménez, C. et al., 2011. Global intercomparison of 12 land surface heat flux estimates. J. Geophys.
833 Res., 116(D2): D02102.

834 Kalma, J., McVicar, T., McCabe, M., 2008. Estimating Land Surface Evaporation: A Review of Methods
835 Using Remotely Sensed Surface Temperature Data. Surveys in Geophysics, 29(4): 421-469.

836 Krishnan, P., Meyers, T.P., Scott, R.L., Kennedy, L., Heuer, M., 2012. Energy exchange and
837 evapotranspiration over two temperate semi-arid grasslands in North America. Agricultural
838 and Forest Meteorology, 153(0): 31-44.

839 Kumar, A. et al., 2011. Evaluation of a Photosynthesis-Based Canopy Resistance Formulation in the
840 Noah Land-Surface Model. Boundary-Layer Meteorology, 138(2): 263-284.

841 Li, L. et al., 2011. Modelling evapotranspiration in a Central Asian desert ecosystem. Ecological
842 Modelling, 222(20–22): 3680-3691.

843 Lokupitiya, E. et al., 2009. Incorporation of crop phenology in Simple Biosphere Model (SiBcrop) to
844 improve land-atmosphere carbon exchanges from croplands. Biogeosciences, 6: 1103 - 1103.

845 McCabe, M.F., Kalma, J.D., Franks, S.W., 2005. Spatial and temporal patterns of land surface fluxes
846 from remotely sensed surface temperatures within an uncertainty modelling framework.
847 Hydrol. Earth Syst. Sci., 9(5): 467-480.

848 McCabe, M.F., Wood, E.F., 2006. Scale influences on the remote estimation of evapotranspiration
849 using multiple satellite sensors. Remote Sensing of Environment, 105(4): 271-285.

850 Montandon, L.M., Small, E.E., 2008. The impact of soil reflectance on the quantification of the green
851 vegetation fraction from NDVI. Remote Sensing of Environment, 112(4): 1835-1845.

852 Monteith, J.L., 1965. Evaporation and environment. Symp. Soc. Exp. Biol., 19: 205-234.

853 Moriasi, D.N. et al., 2007. Model evaluation guidelines for systematic quantification of accuracy in
854 watershed simulations, 50. American Society of Agricultural Engineers, St. Joseph, MI,
855 ETATS-UNIS, 16 pp.

856 Mu, Q., Heinsch, F.A., Zhao, M., Running, S.W., 2007. Development of a global evapotranspiration
857 algorithm based on MODIS and global meteorology data. Remote Sensing of Environment,
858 111(4): 519-536.

859 Mu, Q., Zhao, M., Kimball, J.S., McDowell, N.G., Running, S.W., 2012. A Remotely Sensed Global
860 Terrestrial Drought Severity Index. Bulletin of the American Meteorological Society, 94(1):
861 83-98.

862 Mu, Q., Zhao, M., Running, S.W., 2011. Improvements to a MODIS global terrestrial
863 evapotranspiration algorithm. Remote Sensing of Environment, 115(8): 1781-1800.

864 Mueller, B. et al., 2013. Benchmark products for land evapotranspiration: LandFlux-EVAL multi-
865 dataset synthesis. Hydrol. Earth Syst. Sci. Discuss., 10(1): 769-805.

866 Mueller, B. et al., 2011. Evaluation of global observations-based evapotranspiration datasets and
867 IPCC AR4 simulations. Geophys. Res. Lett., 38(6): L06402.

868 Nash, J.E., Sutcliffe, J.V., 1970. River flow forecasting through conceptual models part I — A
869 discussion of principles. Journal of Hydrology, 10(3): 282-290.

870 Noilhan, J., Planton, S., 1989. A Simple Parameterization of Land Surface Processes for
871 Meteorological Models. Monthly Weather Review, 117(3): 536-549.

872 Ortega-Farias, S., Poblete-Echeverría, C., Brisson, N., 2010. Parameterization of a two-layer model
873 for estimating vineyard evapotranspiration using meteorological measurements. Agricultural
874 and Forest Meteorology, 150(2): 276-286.

875 Penman, H.L., 1948. Natural Evaporation from Open Water, Bare Soil and Grass. Proceedings of the
876 Royal Society of London. Series A. Mathematical and Physical Sciences, 193(1032): 120-145.

877 Raupach, M., Finnigan, J., 1988. Single-layer models of evaporation from plant canopies are incorrect
878 but useful, whereas multilayer models are correct but useless. Functional Plant Biology,
879 15(6): 705-716.

880 Rebmann, C. et al., 2005. Quality analysis applied on eddy covariance measurements at complex
881 forest sites using footprint modelling. Theoretical and Applied Climatology, 80(2-4): 121-141.

882 Richardson, A.D. et al., 2006. A multi-site analysis of random error in tower-based measurements of
883 carbon and energy fluxes. Agricultural and Forest Meteorology, 136(1–2): 1-18.

884 Román, M.O. et al., 2009. The MODIS (Collection V005) BRDF/albedo product: Assessment of spatial
885 representativeness over forested landscapes. Remote Sensing of Environment, 113(11):
886 2476-2498.

887 Ross, J., 1976. Radiative transfer in plant communities. In: Monteith , J.L. (Ed.), Vegetation and the
888 atmosphere. Academic Press, London, pp. 13-56.

889 Scott, R.L., Jenerette, G.D., Potts, D.L., Huxman, T.E., 2009. Effects of seasonal drought on net carbon
890 dioxide exchange from a woody-plant-encroached semiarid grassland. Journal of
891 Geophysical Research: Biogeosciences, 114(G4): G04004.

892 Seneviratne, S.I., Lüthi, D., Litschi, M., Schär, C., 2006. Land–atmosphere coupling and climate
893 change in Europe. Nature, 443(7108): 205-209.

894 Sheffield, J., Wood, E., 2008. Projected changes in drought occurrence under future global warming
895 from multi-model, multi-scenario, IPCC AR4 simulations. Climate Dynamics, 31(1): 79-105.

896 Shuttleworth, W.J., Gurney, R.J., 1990. The theoretical relationship between foliage temperature and
897 canopy resistance in sparse crops. Quarterly Journal of the Royal Meteorological Society,
898 116(492): 497-519.

899 Shuttleworth, W.J., Wallace, J.S., 1985. Evaporation from sparse crops-an energy combination
900 theory. Quarterly Journal of the Royal Meteorological Society, 111(469): 839-855.

901 Simard, M., Pinto, N., Fisher, J.B., Baccini, A., 2011. Mapping forest canopy height globally with
902 spaceborne lidar. Journal of Geophysical Research: Biogeosciences, 116(G4): G04021.

903 Solano, R., Didan, K., Jacobson, A., Huete, A., 2010. MODIS Vegetation Index User's Guide,
904 Vegetation Index and Phenology Lab, The University of Arizona.

905 Stannard, D.I., 1993. Comparison of Penman-Monteith, Shuttleworth-Wallace, and Modified
906 Priestley-Taylor Evapotranspiration Models for wildland vegetation in semiarid rangeland.
907 Water Resour. Res., 29(5): 1379-1392.

908 Stott, P., Paruelo, J.M., Lauenroth, W.K., 1998. Interannual variability of NDVI and its relationship to
909 climate for North American shrublands and grasslands. Journal of Biogeography, 25(4): 721-
910 733.

911 Su, H., McCabe, M.F., Wood, E.F., Su, Z., Prueger, J.H., 2005. Modeling Evapotranspiration during
912 SMACEX: Comparing Two Approaches for Local- and Regional-Scale Prediction. Journal of
913 Hydrometeorology, 6(6): 910-922.

914 Su, Z., 2002. The Surface Energy Balance System (SEBS) for estimation of turbulent heat fluxes.
915 Hydrol. Earth Syst. Sci., 6(1): 85-100.

916 Su, Z., Schmugge, T., Kustas, W.P., Massman, W.J., 2001. An Evaluation of Two Models for Estimation
917 of the Roughness Height for Heat Transfer between the Land Surface and the Atmosphere.
918 Journal of Applied Meteorology, 40(11): 1933-1951.

919 Sulkava, M., Luyssaert, S., Zhehle, S., Papale, D., 2011. Assessing and improving the
920 representativeness of monitoring networks: The European flux tower network example.
921 Journal of Geophysical Research, 116.

922 Tan, B. et al., 2006. The impact of gridding artifacts on the local spatial properties of MODIS data:
923 Implications for validation, compositing, and band-to-band registration across resolutions.
924 Remote Sensing of Environment, 105(2): 98-114.

925 Thom, A.S., 1975. Momentum, mass and heat exchange of the plant communities. In: Monteith , J.L.
926 (Ed.), Vegetation and Atmosphere. Academic Press, London, pp. 57-109.

927 Thornton, P.E., 1998. Regional ecosystem simulation: Combining surface- and satellite-based
928 observations to study linkages between terrestrial energy and mass budgets. 9828151
929 Thesis, University of Montana, United States -- Montana, 280-280 p. pp.

930 Twine, T.E. et al., 2000. Correcting eddy-covariance flux underestimates over a grassland.
931 Agricultural and Forest Meteorology, 103(3): 279-300.

932 van Bavel, C.H.M., Hillel, D.I., 1976. Calculating potential and actual evaporation from a bare soil
933 surface by simulation of concurrent flow of water and heat. Agricultural Meteorology, 17(6):
934 453-476.

935 Veenendaal, E.M., Kolle, O., Lloyd, J., 2004. Seasonal variation in energy fluxes and carbon dioxide
936 exchange for a broad-leaved semi-arid savanna (Mopane woodland) in Southern Africa.
937 Global Change Biology, 10(3): 318-328.

938 Vinukollu, R.K., Wood, E.F., Ferguson, C.R., Fisher, J.B., 2011. Global estimates of evapotranspiration
939 for climate studies using multi-sensor remote sensing data: Evaluation of three process-
940 based approaches. Remote Sensing of Environment, 115(3): 801-823.

941 Wallace, J.S., 1995. Calculating evaporation: resistance to factors. Agricultural and Forest
942 Meteorology, 73(3–4): 353-366.

943 Wang, K., Dickinson, R.E., 2012. A review of global terrestrial evapotranspiration: Observation,
944 modeling, climatology, and climatic variability. Rev. Geophys., 50(2): RG2005.

945 Wharton, S., Schroeder, M., Paw U, K.T., Falk, M., Bible, K., 2009. Turbulence considerations for
946 comparing ecosystem exchange over old-growth and clear-cut stands for limited fetch and
947 complex canopy flow conditions. Agricultural and Forest Meteorology, 149(9): 1477-1490.

948 Wolfe, R.E. et al., 2002. Achieving sub-pixel geolocation accuracy in support of MODIS land science.
949 Remote Sensing of Environment, 83(1–2): 31-49.

950 Zhang, B., Kang, S., Li, F., Zhang, L., 2008. Comparison of three evapotranspiration models to Bowen
951 ratio-energy balance method for a vineyard in an arid desert region of northwest China.
952 Agricultural and Forest Meteorology, 148(10): 1629-1640.

953 Zhang, Y. et al., 2010. Using long-term water balances to parameterize surface conductances and
954 calculate evaporation at 0.05° spatial resolution. Water Resour Res, 46(5): W05512.

955 Zhao, M., Heinsch, F.A., Nemani, R.R., Running, S.W., 2005. Improvements of the MODIS terrestrial
956 gross and net primary production global data set. Remote sensing of Environment, 95(2):
957 164-176.

958 Zhou, M.C. et al., 2006. Estimating potential evapotranspiration using Shuttleworth–Wallace model
959 and NOAA-AVHRR NDVI data to feed a distributed hydrological model over the Mekong River
960 basin. Journal of Hydrology, 327(1–2): 151-173.

961 Zotarelli, L., Dukes, M.D., Morgan, K.T., 2010. Interpretation of Soil Moisture Content to Determine
962 Soil Field Capacity and Avoid Over-Irrigating Sandy Soils Using Soil Moisture Sensors.

963

964

965 **Impact of model structure and parameterization on Penman-Monteith type**

966 **evaporation models**

967 # 6 List of Figures

968

985

Figure 4: Performance of the Mu model in response to adjusting the resistance parameterization. *RE* is relative error and *NSE* is the Nash-Sutcliff efficiency, with each point showing the overall statistic for a particular tower. The x-axis displays the various biomes, with towers in each biome arranged from left to right (e.g. G1 to G4 for grassland). The numbers at the bottom of the *NSE* plot reflect the average NSE (i.e. NSE_{avg}) of the different scenarios for each biome type.

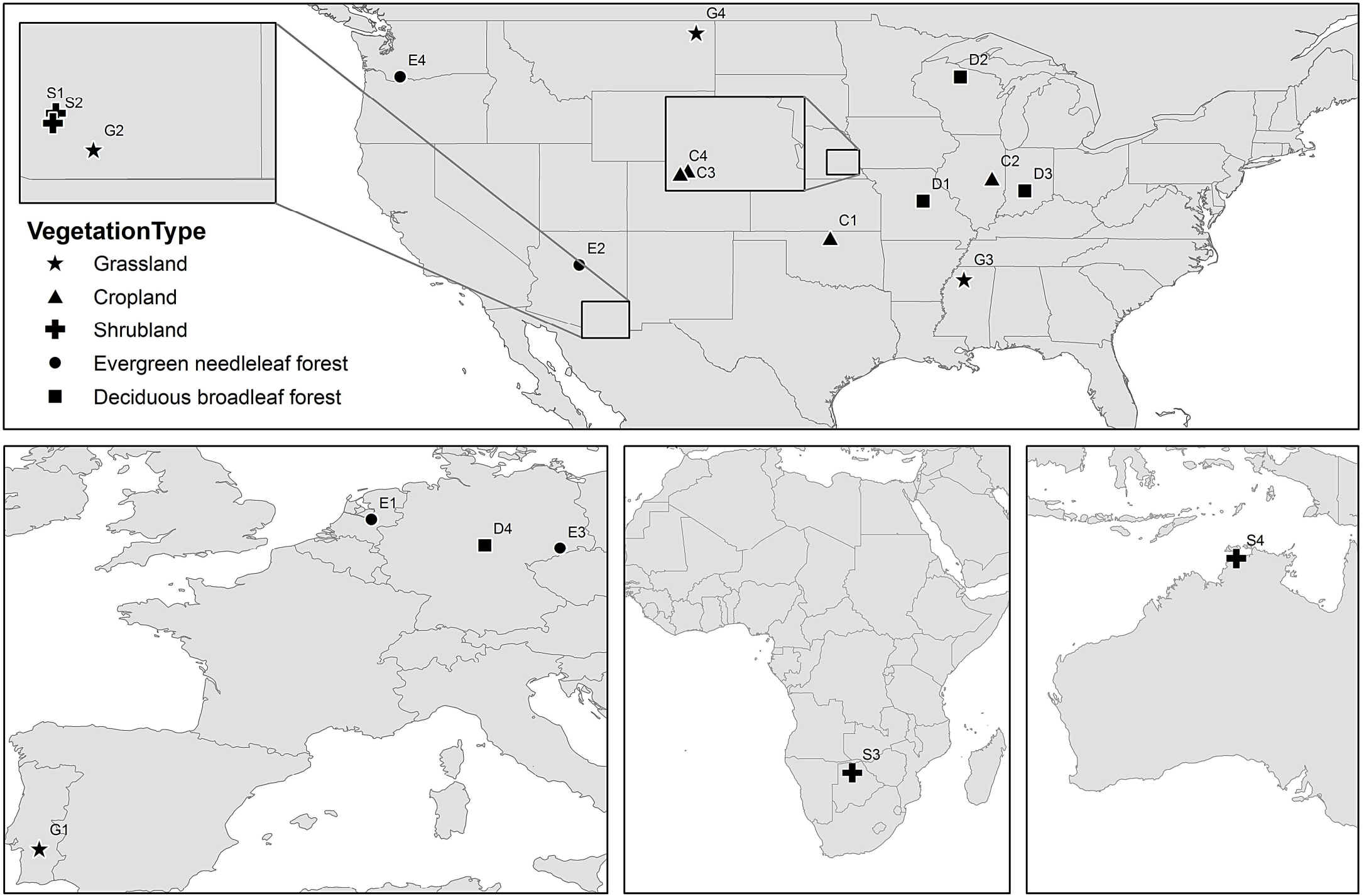
G4
E4
D2
S1
S2
G2
C4
C3
C2
D3
D1
C1
E2
G3
VegetationType
Grassland
Cropland
Shrubland
Evergreen needleleaf forest
Deciduous broadleaf forest
E1
D4
E3
G1
S3
S4

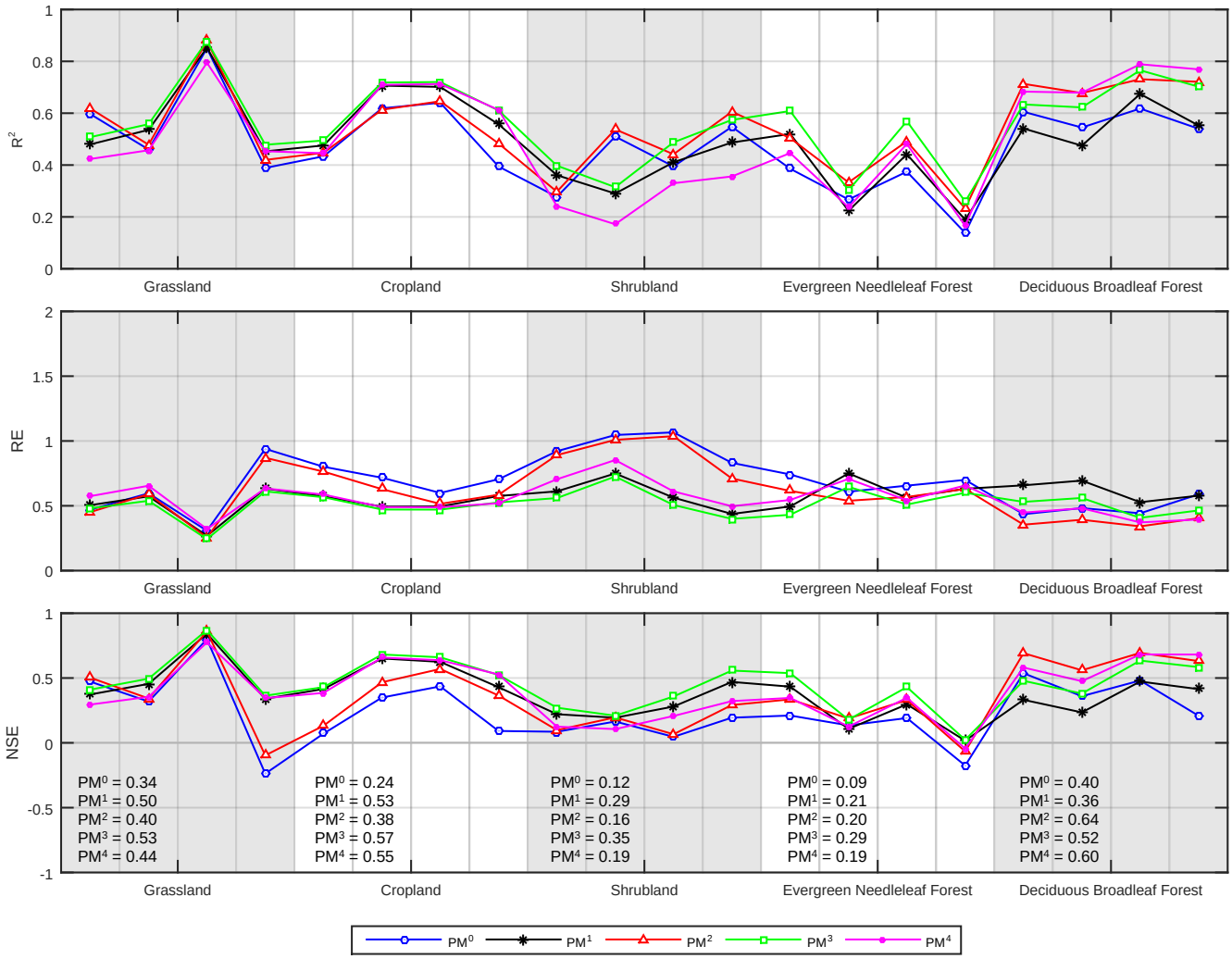

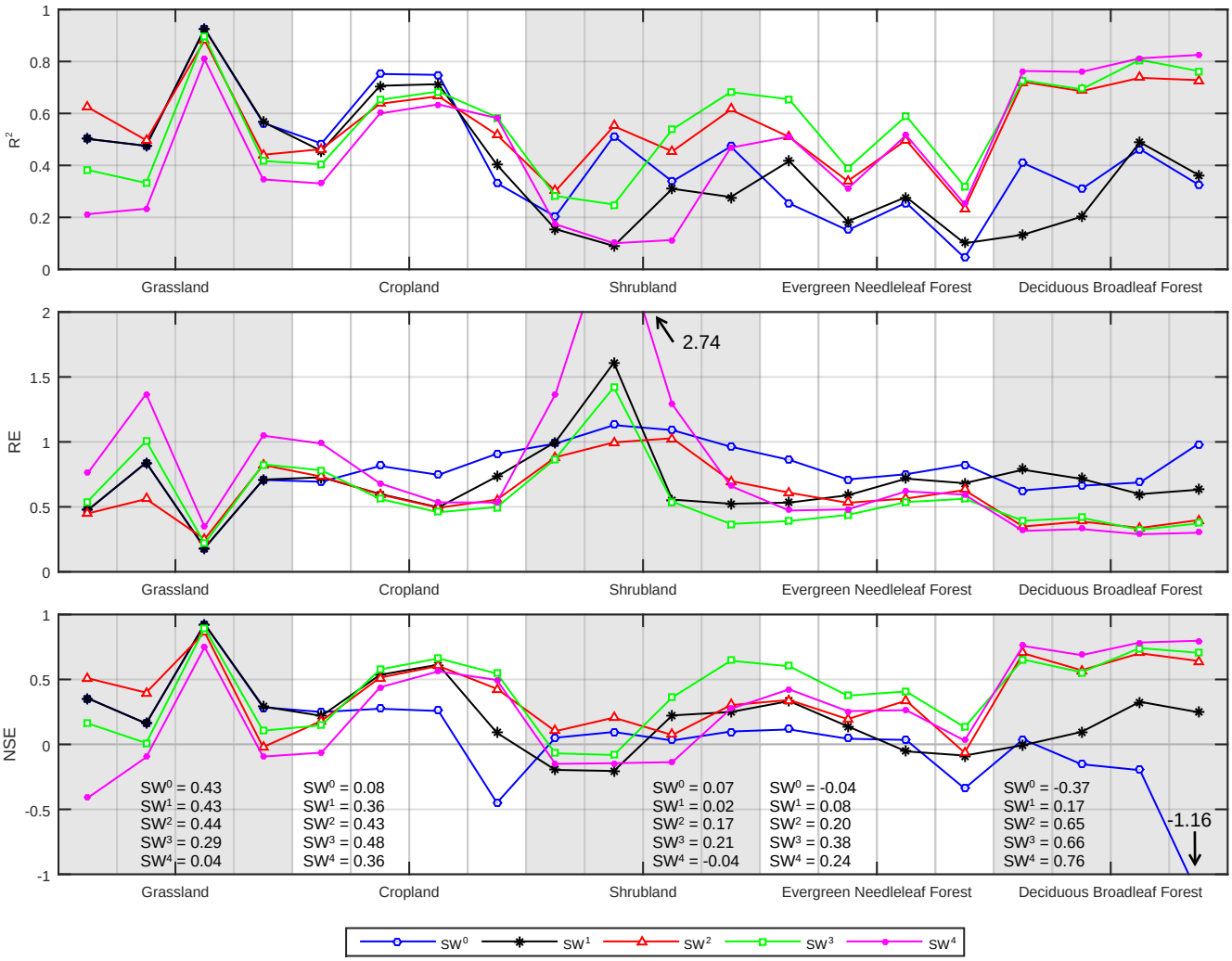

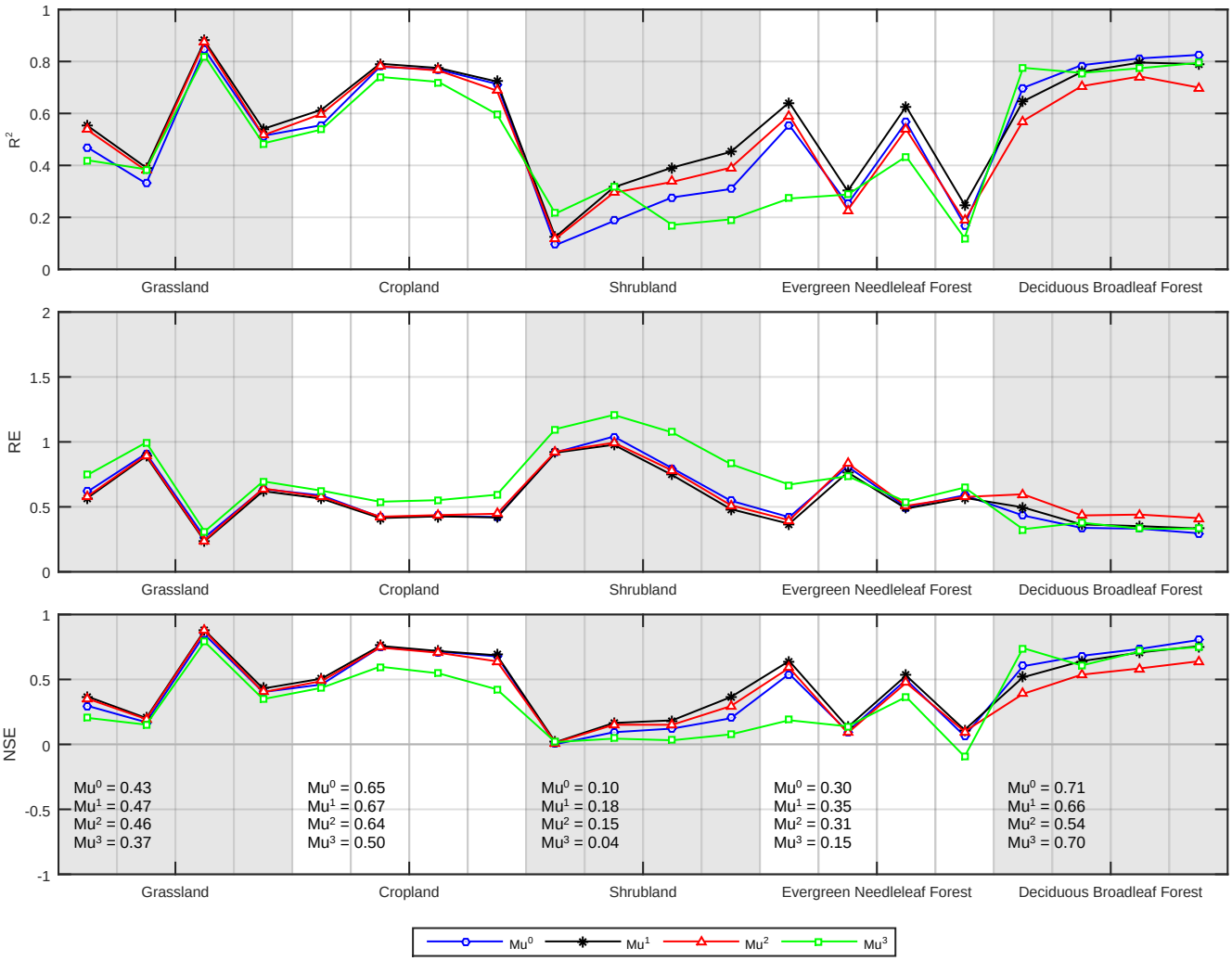

999 Highlights

1000 • Evaluated three Penman-Monteith type models with multi-year data from 20 flux towers
1001 over 5 biomes
1002 • Fourteen unique model configurations were developed to identify impact of resistance
1003 schemes
1004 • No particular model configuration consistently outperformed others
1005 • Considerable model variability was observed both within and between different biomes
1006 • Results provide guidance on model selection and performance across typical biome types
1007

1008